Transcriptome-based screening of ion channels and transporters in a migratory chondroprogenitor cell line isolated from late-stage osteoarthritic cartilage

Csaba Matta (matta.csaba@med.unideb.hu)
University of Debrecen https://orcid.org/0000-0002-9678-7420

Rebecca Lewis
University of Surrey https://orcid.org/0000-0003-1395-3276

Christopher Fellows
University of Surrey

Gyula Diszhazi
University of Debrecen

Janos Almassy
University of Debrecen

Nicolai Miosge
Georg August University

James E. Dixon
University of Nottingham

Marcos C. Uribe
University of Nottingham

Sean May
University of Nottingham

Szilard Poliska
University of Debrecen

Richard Barrett-Jolley
University of Liverpool https://orcid.org/0000-0003-0449-9972

Erin Henslee
University of Surrey

Fatima H. Labeed
University of Surrey https://orcid.org/0000-0002-0092-257X

Michael P. Hughes
University of Surrey

Ali Mobasheri
University of Oulu https://orcid.org/0000-0001-6261-1286

Research Article

Keywords: Chondrocyte, Cartilage, Mesenchymal stem cell, Osteoarthritis, Chondroprogenitor, Transcriptomics, Channelome

Posted Date: November 13th, 2020

DOI: https://doi.org/10.21203/rs.3.rs-106355/v1

Version of Record: A version of this preprint was published at Journal of Cellular Physiology on May 18th, 2021. See the published version at https://doi.org/10.1002/jcp.30413.

Abstract

Chondrogenic progenitor cells (CPCs) may be used as an alternative source of cells with potentially superior chondrogenic potential compared to mesenchymal stem cells (MSCs), and could be exploited for future regenerative therapies targeting articular cartilage in degenerative diseases such as osteoarthritis (OA). In this study, we hypothesised that CPCs derived from OA cartilage may be characterised by a distinct channelome. First, a global transcriptomic analysis using Affymetrix microarrays was performed. We studied the profiles of those ion channel and transporter families that may be relevant to chondroprogenitor cell physiology. Following validation of the microarray data, we examined the role of calcium-dependent potassium channels in CPCs and observed functional large conductance calcium-activated potassium channels (BK) involved in the maintenance of chondroprogenitor phenotype. In line with our very recent results, we found that the KCNMA1 gene was upregulated in CPCs and observed currents that could be attributed to the BK channel in both cell types. Through characterisation of their channelome we demonstrate that CPCs are a distinct cell population but are highly similar to MSCs in many respects. This work adds key mechanistic data to the in-depth characterisation of CPCs and their phenotype in the context of cartilage regeneration.

List Of Abbreviations

AD-MSC, adipose tissue-derived mesenchymal stem cell; BK; large conductance calcium-activated potassium channel; BM-MSC, marrow-derived mesenchymal stem cell; CPC, chondrogenic progenitor cell; CRAC; Ca^{2+} release-activated Ca^{2+} channel; DEP, dielectrophoresis; ECM, extracellular matrix; ENaC; epithelial sodium channel; GAG, glycosaminoglycan; IBTX, iberiotoxin; MSC, mesenchymal stem cell; OA, osteoarthritis; Pax, paxilline; PCA, principal component analysis; PG, proteoglycan; RMP, resting membrane potential; SOCE, store-operated Ca^{2+} entry; TRP, transient receptor potential

Introduction

The prevalence of musculoskeletal conditions is constantly increasing, making age-related and chronic inflammatory joints diseases the major causes of disability in the elderly population (Al Maini et al., 2020). Osteoarthritis (OA) is the most common form of chronic musculoskeletal disorders (Hunter & Bierma-Zeinstra, 2019). Although the primary target of OA is articular cartilage, it also affects other tissues within and around the joint (Loeser, Goldring, Scanzello, & Goldring, 2012). The affected tissues undergo metabolic, structural and functional alterations that contribute to joint pain, disease progression, and eventually lead to patient disability (Henrotin, Sanchez, Bay-Jensen, & Mobasheri, 2016).

Chondrocytes are the main cell type in articular cartilage (Archer & Francis-West, 2003), along with a scarce population of cartilage progenitor cells (CPCs) (Nakayama et al., 2020). The resident cells are embedded in a cartilage-specific extracellular matrix (ECM) that consists of collagen type II, large

aggregating proteoglycans (PGs; e.g. aggrecan), constituent glycosaminoglycans (GAGs), hyaluronan, small PGs, and other collagenous and non-collagenous proteins (Buckwalter, Mankin, & Grodzinsky, 2005). A high amount of interstitial water (approximately 80% of total weight of cartilage) is osmotically drawn to the freely mobile cations (i.e. Na^+, K^+, Ca^{2+}) balancing the negatively charged GAG side chains of PGs and are therefore present at high local concentrations. Cells in cartilage ECM are therefore exposed to a unique ionic micro-environment (Mobasheri et al., 1998; Urban, Hall, & Gehl, 1993). Cartilage is avascular, and as a consequence of the scarcity of available nutrients and oxygen, as well as its unique, relatively hypoxic and acidic milieu, it is incapable of mounting a sufficient healing and repair response following injury (Gomoll & Minas, 2014).

The presence of a cartilage-specific CPC population with stem cell properties in the superficial zone of articular normal cartilage is now widely accepted (Dowthwaite et al., 2004). More recently, cells in OA articular cartilage with mesenchymal progenitor cell characteristics have also been observed and characterised (Fellows et al., 2017). These cartilage progenitor/stem cell populations have the potential for chondrogenic induction and tri-lineage plasticity. CPCs in late-stage OA cartilage have also been described, which are believed to be migrating in response to chemotactic signals from the bone marrow through breaks in the tide mark as an attempt to regenerate damaged cartilage ECM (Koelling et al., 2009). However, knowledge concerning the specific phenotypic features and regenerative potentials of the chondroprogenitor cells is still incomplete. CPCs are considered an ideal source for cell-based cartilage repair, and therefore progress has been made in identifying, understanding, and characterizing these cells.

In OA, chondrocytes and CPCs exist in a micro-environment dominated by mediators that promote matrix degradation and low-grade inflammation. There is evidence that cartilage ECM undergoes profound alterations during OA in terms of GAG and water content (Mankin & Lippiello, 1970). That in turn alters the osmolality of the matrix and the composition of the unique ionic milieu (Mow, Wang, & Hung, 1999). Chondrocytes and other cells in cartilage respond to these changes and maintain their homeostasis by altering the transport of ions across the cell membrane (Hdud, Mobasheri, & Loughna, 2014) via a range of transporters and ion channels, collectively referred to as the ‘channelome’ (Asmar, Barrett-Jolley, Werner, Kelly, & Stacey, 2016; Barrett-Jolley, Lewis, Fallman, & Mobasheri, 2010; Mobasheri et al., 2019).

Plasma membrane transporters including voltage-gated sodium, potassium and calcium channels, chloride channels, calcium-activated potassium channels, transient receptor potential (TRP) channels, N-methyl-D-aspartate (NMDA) receptors and purinergic receptors have been described in chondrocytes, which allow them to respond to the local ionic composition of the pericellular matrix by adjusting the resting membrane potential (RMP) (Maleckar, Martin-Vasallo, Giles, & Mobasheri, 2020), which has been shown to play a crucial role in regulating metabolic activity and synthetic rate of cartilage ECM, as well as proliferation, differentiation, or volume regulation (Asmar et al., 2016; Matta & Zakany, 2013; Mobasheri et al., 2019). Although much progress has been made towards characterising the chondrocyte channelome, many open questions remain concerning the composition of the ion channel complement and their function in both chondroprogenitor cells and mature chondrocytes. Whilst there is accumulating data

suggesting that several genes encoding ion channels which are involved in the regulation of mechanotransduction, cell volume, RMP, and apoptosis are differentially expressed in OA chondrocytes (Lewis & Barrett-Jolley, 2015), current understanding concerning the channelome of CPCs, especially with regards to differentially regulated ion channel genes, is incomplete. Addressing this gap in knowledge is high priority for identification and targeting of new therapeutic targets for the treatment of OA.

In this study we hypothesised that CPCs derived from OA cartilage may be characterised by a different assembly of ion channels and transporters that regulate their function and phenotype, and maintain communication with the altered ECM. Given that there is some evidence that migratory CPCs are related to MSCs residing in the bone marrow close to the subchondral bone which have migrated to lesioned cartilage through breaks in the tide mark, we used bone marrow-derived MSCs (BM-MSCs) as a reference cell population. We have recently analysed the surfaceome of CPCs using selective cell surface protein labelling followed by quantitative high-throughput mass spectrometry and identified alterations in the composition of the surfaceome compared to MSCs (Matta et al., 2019). However, even that approach was not sensitive enough to detect alterations in very low-abundance ion channels or other transporters. In this study, we attempted to differentiate CPCs from BM-MSCs based on their transcriptome and electrophysiological properties. We first performed a global transcriptomic analysis using Affymetrix microarrays. We studied the profiles of those ion channel and transporter families that are known to be involved in regulating chondrocyte physiology, RMP, volume regulation, calcium signalling, matrix secretion, or chondrogenesis, which may have a relevance in chondroprogenitor cell physiology (Barrett-Jolley et al., 2010; Matta & Zakany, 2013; Mobasheri et al., 2019; Suzuki, Yamamura, Imaizumi, Clark, & Giles, 2020). We then employed patch clamping and dielectrophoresis to characterise the basic electrophysiological profile (the ‘electrome’ (De Loof, 2016)) of the two cell types. Following validation of the microarray data using RT-qPCR, we examined the role of calcium-dependent potassium channels in the cellular physiology and homeostasis of migratory CPCs and found that the large conductance calcium-activated potassium channels (BK) are functionally expressed and are involved in the maintenance of the chondroprogenitor phenotype.

Materials And Methods

1. *Cell cultures*

Experiments were carried out on a human migratory CPC cell line derived from late-stage OA knee articular cartilage, which has been immortalised by viral transfection of the human telomerase reverse transcriptase (hTERT) as previously described (Koelling et al., 2009). CPCs were cultured in monolayers in 75 cm^2 cell culture flasks (Nunc, Thermo Fisher Scientific, Waltham, MA, USA) until ~80% confluence in GlutaMax DMEM (1.0 g/L glucose; Gibco, Thermo Fisher Scientific) containing 10% FCS (foetal calf serum; Gibco) and 50 µg/mL gentamycin (Sigma-Aldrich, St. Louis, MO, USA). As a reference cell population, human BM-MSCs (Lonza, Basel, Switzerland) were used. The cells were received at passage 2 and were expanded until passage 4 in Lonza hMSC medium at 37°C in a humidified atmosphere of 5% CO_2. MSCs were hTERT-immortalised as previously described in (Okamoto et al., 2002) with the

modifications detailed in (Saeed et al., 2015). Immortalised MSCs were expanded in monolayers in 75 cm^2 cell culture flasks (Nunc) until ~80% confluence in GlutaMax DMEM (4.5 g/L glucose; Gibco) containing 10% FCS (Gibco) and 1% P/S (Sigma-Aldrich).

2. *RNA isolation and reverse transcription*

Total RNA was isolated from cells grown in monolayers in 75 cm^2 cell culture flasks using the RNeasy kit (Qiagen, Hilden, Germany) as per the instructions of the manufacturer, and stored at −80°C. RNA concentration and purity was determined by a Nanodrop 2000 UV-Vis spectrophotometer (Thermo Fisher Scientific). For gene expression analyses, 2000 ng of RNA was reverse transcribed into complementary cDNA using the High-Capacity cDNA Reverse Transcription Kit (Thermo Fisher Scientific), following the protocol supplied by the manufacturer. cDNA was stored at −20°C.

3. *Affymetrix microarray analysis*

RNA integrity was confirmed using an Agilent 2100 Bioanalyzer with the RNA 6000 Nano Kit (Agilent Technologies, Palo Alto, CA). The RNA integrity numbers (RIN) were ≥ 9.6 for all samples. Whole-genome transcriptome analysis was conducted by hybridising three biological samples of total RNA per cell type to Affymetrix Human Gene 2.1 ST Arrays Strips (Affymetrix, Santa Clara, CA, USA). All steps were conducted at the Nottingham Arabidopsis Stock Centre. Gene expression data were analysed using Partek Genomics Suite 6.6 software (Partek Incorporated, St. Louis, MO, USA). The raw CEL files were normalised using the RMA background correction with quantile normalisation, log base 2 transformation and mean probe-set summarisation with adjustment for GC content. Differentially expressed genes (DEG) were identified by a two-way ANOVA, and *P*-values were adjusted using the false-discovery rate (FDR) method to correct for multiple comparisons. DEG were considered significant if *P*-value with FDR was ≤ 0.05. The data set is published in a MIAME compliant format in the GEO database (http://www.ncbi.nlm.nih.gov/geo/); accession numbers: GSM4885525-GSM4485530.

4. *Pathway analysis*

CytoScape v3.4 software with ClueGo v2.3.5 application was used for identifying over- represented Gene ontology (GO) terms. Two-sided hypergeometric test with Bonferroni step down correction was performed using the list of differentially expressed genes and the GO Biological process database.

5. *Quantitative real-time polymerase chain reaction (RT-qPCR) analyses*

The mRNA expression of candidate genes encoding various ion channel subunits were first validated using custom configured TaqMan 96-Well Fast Gene Expression Array plates (Design ID: PP0OXUF; Thermo Fisher Scientific) using TaqMan Gene Expression Master Mix (Thermo Fisher Scientific) and 50 ng of input cDNA per 10-µL reactions on a QuantStudio 7 Flex Real-Time PCR System (Thermo Fisher Scientific) platform. The plate map is supplied in Table S1 in the Supporting information. The plates were set up according to the instructions of the manufacturer. The thermal cycling conditions were set as follows: hold at 50°C for 2 minutes, then denaturation at 95°C for 2 minutes, followed by 40 cycles of 95°C for 15 seconds and 60°C for 60 seconds. Data were analysed using the double delta Ct method; gene expression data were normalised to *PPIA*, the most stably expressed reference gene.

Selected ion channel subunit genes were further analysed by RT-qPCR by absolute quantification using the standard curve method. Primer pairs were ordered from Eurogentec (Liège, Belgium). For sequences of primer pairs please see Table S2 in the Supporting information. First, standard curves had been generated by conventional PCR using the Promega GoTaq Flexi DNA Polymerase kit (Promega, Madison, WI, USA) by adding the following components (per 50 µL reaction): 1.25 U GoTaq polymerase; 3 mM $MgCl_2$; 0.2 mM dNTP; 200 nM primers; and 10 ng cDNA. Amplification was performed in a Techne Prime Thermal Cycler (Techne, Bibby Scientific Ltd, Stone, UK) using the following thermal profile: initial denaturation at 95°C for 5 minutes, followed by 40 cycles of denaturation at 95°C for 15 sec, annealing at 58°C for 20 sec, extension at 74°C for 20 sec, and then final extension at 74°C for 5 minutes. PCR products were isolated using a Roche High Pure PCR Product Purification Kit (Roche, Basel, Switzerland) according to the instructions of the manufacturer. DNA concentration of purified PCR products was determined using a Nanodrop 2000 UV-Vis spectrophotometer (Thermo Fisher Scientific). Standard curves were prepared by a serial (10-fold) dilution starting from 1 ng/µL.

RT-qPCR reactions were set up using the Promega GoTaq qPCR Master Mix and 20 ng input cDNA per each 10-µL reaction. Reactions were run in a Techne Prime Pro 48 Real-time qPCR machine using the following thermal profile: activation and initial denaturation at 95°C for 10 minutes, followed by 40 cycles of denaturation at 95°C for 10 sec, annealing at 58°C for 30 sec, extension at 72°C for 20 sec, and then final extension at 72°C for 20 sec. Quantification of qPCR products was performed by absolute quantification using the standards prepared in the previous step, followed by normalising the expressional data of genes of interest to those of the most stably expressed reference gene (*PPIA*). The optimal normalization gene was selected using the NormFinder algorithm (Andersen, Jensen, & Orntoft, 2004). RT-qPCR reactions were performed on 3 biological replicates.

6. *Electrophysiology*

6.1. Dielectrophoresis

Cells were grown to ~80% confluence before analysis. Cells were dissociated from the culture plates by trypsinisation. Afterwards, cells were washed twice and resuspended in an iso-osmotic DEP medium with

low ionic strength containing 8.5% (w/v) sucrose (Sigma-Aldrich, St. Louis, MO, USA), 0.3% (w/v) glucose (Sigma-Aldrich), and adjusted to a final conductivity of 10 mS/m using phosphate buffered saline (PBS; Sigma-Aldrich). Buffer conductivity was measured with a conductivity meter (RS components Ltd, London, UK). Cell counts and viability for each experiment were determined using a haemocytometer and trypan blue, which indicated a 96% ± 2% viability. To reduce the effect of variation in cell numbers in each sample, the final cell concentration was adjusted to 5×10^5 cells/mL.

DEP spectra were obtained using the 3DEP DEP-Well system (Deptech, UK), as described in more detail earlier (Labeed et al., 2011). Briefly, cells resuspended in DEP media were administered into the wells of DEP-Well chips containing 12 ring-shaped, 17 μm wide, gold-plated copper electrodes around the well circumference with gaps of 75 μm between electrodes, and energised with currents at specific frequencies. The DEP method is based on the principle that the cells are either attracted or repelled from the side of the well by an amount proportional to their polarizability, as described previously (Hoettges et al., 2019).

Changes in light intensity across the wells over time were determined using a 1.3 Mpixel video camera installed on the microscope and a Matlab (Mathworks Inc, Natick, MA, USA) script. The change in cell distribution was monitored by recording an image every 3 s for a total of 30 s. The entire well was divided into 10 segments that were monitored separately; however, only segments 7–9 were analysed as previously described (Hoettges et al., 2008). The wells were energised with frequencies ranging from 1 kHz–20 MHz at 5 points per decade. Spectra were generated using Matlab (Mathworks, Natick, USA), and presented in values of light intensity versus frequency. Using Matlab, light intensity data were fit to the single shell model (Broche, Labeed, & Hughes, 2005) and the best-fit model was used to determine the following features: specific membrane capacitance (C_{spec}), specific membrane conductance (G_{spec}), and crossover frequency (i.e. the frequency where the DEP force is zero). The best-fit model (highest Pearson correlation coefficient) was established by matching the curve to the measured data and adjusting the dielectric cytoplasmic and membrane parameters until the best match was found. Matlab scripts were used for all images as well as for signal processing and data analysis as previously described (Hoettges et al., 2008). Given that the key parts of the DEP curve (starting and end values and transition frequencies) can be associated with the membrane capacitance and conductance, and cytoplasm conductivity and permittivity, these parameters were determined uniquely by fitting the curve to the data points. Cell diameters were measured in a haemocytometer and the average radius was calculated using ImageJ software version 1.51 (http://imagej.nih.gov/ij/); the mean radii were used for the DEP model. All experiments were repeated three times; data are expressed as mean ± standard deviation (SD).

6.2. Patch clamp

Whole cell currents were measured under voltage clamp conditions as described earlier (Almassy & Begenisich, 2012). Extracellular solution contained (in mM): NaCl, 140; KCl, 5; $CaCl_2$, 2; $MgCl_2$, 1; HEPES,

10; glucose, 5; pH 7.4 with NaOH. Patch pipettes were fabricated from thick-walled borosilicate glass (o.d. 1.5 mm, i.d. 0.85 mm) with resistance of approximately 5MΩ when filled with intracellular solution. The pipette solution contained (in mM): D-gluconic acid potassium salt, 115; KCl, 26; $MgCl_2$, 1; EGTA, 5; HEPES, 10; pH 7.2 with KOH. The specific BK channel inhibitor paxilline (Alomone Labs, Jerusalem, Israel) was used in 5 μM to verify the functional expression of the channels. V_m values were determined following 2 minutes of stable membrane potential recording with I = 0 on Axon 200A/B amplifiers (Lewis et al., 2011). Only cells with seal resistance above 10 GΩ and good access (Rs < 20) were used. All values are quoted as mean ± SEM, with sample size = 22 (CPC) and 8 (MSC). All membrane potentials are corrected for liquid junction potentials estimated using JPCalc (Barry & Lynch, 1991).

7. *Cell proliferation and mitochondrial activity assays*

To assess the effect of BK channel modulators, cells were plated into 96-well plates at a density of 5,000 cells/well. Prior to the assays, cells were incubated for 48 h in the presence of the selective BK channel blocker iberiotoxin (100 nM; Tocris, Bio-Techne, Minneapolis, MN, USA); the potent BK channel inhibitor paxilline (1 μM); the BK channel activator NS1619 (10 μM; Sigma-Andrich); or vehicles at equal volumes (water, DMSO and ethanol, respectively). Rate of cell proliferation was determined by detecting the amount of incorporated radioactivity from ^{3}H-thymidine. 1 μCi/mL ^{3}H-thymidine (diluted from methyl-^{3}H-thymidine; 185 GBq/mM, Amersham Biosciences, Budapest, Hungary) was added to each well (Wallac, PerkinElmer Life and Analytical Sciences, Shelton, CT, USA) for 24 h. After washing with PBS, proteins were precipitated with ice-cold 5% trichloroacetic acid, and rinsed with PBS again. Cells were then air-dried and radioactivity was counted by a liquid scintillation counter (Chameleon, Hidex, Turku, Finland). Measurements were carried out in 7 samples of each experimental group in 3 independent experiments. For mitochondrial activity assays, 10 μL MTT reagent (thiazolyl blue tetrazolium bromide; 5 mg MTT/1 mL PBS; Sigma-Aldrich) was pipetted into each well. Cells were incubated for 2 h at 37°C, and following the addition of 500 μL MTT solubilizing solution, optical density was measured at 570 nm (Chameleon, Hidex).

8. *Statistical analysis*

All data are representative of at least three independent experiments (biological replicates). RT-qPCR, as well as cell proliferation and mitochondrial activity data are expressed as mean ± SEM and statistical analysis was performed using Student's unpaired two-tailed *t*-test (*P < 0.05).

Results

1. *Affymetrix analysis reveals differentially expressed ion channel genes in migratory CPCs*

We performed principal component analysis (PCA) of the Affymetrix data on normalized samples to explore their interrelationships (Fig. 1). Biological replicates within the CPC/MSC groups were separated into two distinct clusters, showing that the pattern of gene expression was different in CPC and MSC. In total, 3214 genes showed significantly different expression levels between CPC and MSC cells, with 2379 genes being down-regulated and 835 genes up-regulated. Using CytoScape software with the ClueGo application we identified those GO Biological process terms which were over-represented in our gene list. When we analysed the full gene list (up and down-regulated genes together), and the list of down-regulated genes, we found that mainly cell cycle-related categories such as cell cycle, regulation of cell cycle, cell cycle checkpoint, and mitotic/meiotic cell cycle processes were enriched. Furthermore, DNA/nucleic acid metabolism-related pathways were also overrepresented. Separate analyses of up-regulated genes indicated the enrichment of different type of tissue development and cell proliferation processes, such as skin development and mesenchymal cell proliferation (Fig. 2; see also Figure S1 in the Supporting Information).

To characterise the expression profiles of genes encoding ion channel subunits in CPCs and to identify differences in expression levels compared to MSCs, we further explored the microarray analysis data. We assessed genes encoding ion channels and transporters commonly involved in regulating potassium, sodium and chloride transport, and calcium homeostasis in chondrocytes (Tables 1-4, Fig. 3). The expression levels for some of the genes studied were different in migratory CPCs *vs*. MSCs. Genes encoding members of the calcium-activated potassium channels (K_{Ca}) showed the most prominent expression changes; *KCNMA1* and *KCNN4*, the genes coding for the pore forming alpha subunit of the large conductance calcium-activated potassium channel ($K_{Ca}1.1$), and the intermediate/small conductance calcium-activated potassium channel ($K_{Ca}3.1$), respectively. In both cases, there was a more than 1.5-fold upregulation in CPCs (*KCNMA1*, 1.67-fold upregulation, $P = 0.016$; *KCNN4*, 1.62-fold upregulation, $P = 0.033$). In contrast, the small conductance calcium-activated potassium channel ($K_{Ca}2.3$) encoded by the *KCNN3* gene showed a small but non-significant downregulation (FC = −1.12, $P = 0.132$). The β4 regulatory subunit of the large conductance calcium-activated potassium channel (*KCNMB4*) was significantly downregulated in CPCs (FC = −1.05; $P = 0.024$) (Table 1). *KCNB1* (voltage-gated potassium channel subunit Kv2.1); *KCND2* (Kv4.2) and *KCNH6* (Kv11.2) were also downregulated in CPCs (FC = −1.21, −1.65 and 1.17; $P = 0.048$, 0.024 and 0.037, respectively).

Whilst most of the genes coding for the alpha subunits of voltage-gated sodium channels were also upregulated in CPCs, with *SCN2A* encoding the $Na_V1.2$ sodium channel showing a 1.3-fold upregulation ($P = 0.027$), all epithelial sodium channel (ENaC) subunit genes (*SCNN1A*, *SCNN1B*, *SCNN1D*, *SCNN1G*) were found to show a trend towards downregulation (Table 2), suggesting an altered K^+/Na^+ ion handling in CPCs. The only gene showing a significantly lower expression in CPCs was *SCNN1D* (FC = −1.16; $P = 0.022$).

Interesting differences were also found in the expression patterns of genes coding for proteins involved in global calcium handling. The genes coding for molecules that regulate store-operated calcium entry

(SOCE); inositol 1,4,5-trisphosphate receptors (IP_3Rs) that mediate calcium release from the intracellular calcium stores; as well as the sarcoplasmic/endoplasmic reticulum Ca^{2+} ATPase (SERCA) that are responsible for calcium sequestration were showing a trend for downregulation in CPCs. Transcript levels of both *ORAI2* and *ATP2A3* (sarcoplasmic/endoplasmic reticulum calcium ATPase 3) showed a 1.46-fold reduction in CPCs ($P = 0.008$ and 0.048, respectively). In contrast, genes coding for voltage-gated calcium channel subunits were unchanged. In a similar way, the ATPases and exchangers that mediate calcium extrusion (*PMCA2-4*, as well as *NCX1-2*); as well as the metabotropic purinergic receptors were also unchanged with a trend towards upregulation, with the exception of *P2Y2*, which was significantly downregulated in CPCs (FC = −1.57; $P = 0.003$). The genes coding for nonselective cation channels, including members of the ionotropic P2X purinergic receptors, as well as the transient receptor potential cation channel families TRPC and TRPV were showing a general trend towards downregulation, in particular *TRPC4* (FC = −1.64; $P = 0.008$) and *TRPV2* (FC = −1.79; $P = 0.015$) (Table 3).

We have also looked at other ion channel expression patterns and found that the only gene which had a significantly different expression (downregulation in CPCs) between the two cell types was *ASIC1* coding for the acid-sensitive cation channel subunit 1 (FC = −1.29, $P = 0.005$). None of these transcripts showed significantly different expression levels between CPCs and MSCs (Table 4).

2. *Validating microarray data by RT-qPCR confirmed the differential expression of ion channel genes in CPCs*

The mRNA expression profiles of selected candidate genes encoding various ion channel subunits were first validated using custom-configured TaqMan 96-Well Fast Gene Expression Array plates. Gene expression data were normalised to *PPIA*, the most stably expressed reference gene. Transcripts of most, but not all candidate genes were confirmed using the qPCR array plates, but the expression patterns were in some cases contrary to those observed on the microarrays (Table 5). Given their role in chondroprogenitor and chondrocyte physiology, we were particularly interested in studying the roles of the calcium-activated potassium channels, we looked at the expression patterns of the genes encoding the various subunits of these channels in details. We confirmed mRNA expression of *KCNMA1*, the gene coding for the α subunit of the large conductance calcium-activated potassium channel, all four β subunits (*KCNMB1–4*), as well as that of the small conductance calcium-activated potassium channel proteins 1–3 (*KCNN1–3*), and the intermediate conductance calcium-activated potassium channel protein 4 (*KCNN4*). Whilst *KCNMA1* was also found to be unregulated in CPCs (FC = 1.95; $P = 0.04$), *KCNMB4* was showing a massively decreased expression in the chondroprogenitors (FC = −25.82; $P = 0.01$).

To confirm the expression patterns of these genes, we employed custom-designed primers and performed individual qPCR reactions. The genes coding for the α and β subunits of the large conductance calcium-activated potassium channel (BK) were all detected; *KCNMA1* was upregulated (FC = 2.49; $P = 0.001$);

KCNMB1 was downregulated in CPCs (FC = −5.88; $P = 0.007$); *KCNMB2, KCNMB3* and *KCNMB4* were unchanged (FC = −2.3, $P = 0.18$; FC = 1.3, $P = 0.19$; FC = 3.64, $P = 0.011$, respectively). Of the genes encoding the small conductance calcium-activated potassium channel proteins 1–3 (*KCNN1–3*), *KCNN1* was unchanged (FC = 1.71; $P = 0.12$), whereas *KCNN3* was massively downregulated in CPCs (FC = −13.23; $P < 0.001$). The gene for the intermediate conductance calcium-activated potassium channel protein 4 (*KCNN4*) was showing a significant downregulation in CPCs (FC = −2.59; $P < 0.001$) (Fig. 4).

3. *Modulation of the BK potassium channel alters cell proliferation*

To assess the role of large conductance calcium-activated potassium channels in CPCs and MSCs on cell proliferation and viability (mitochondrial activity), cells were incubated in the presence of the selective BK channel inhibitors iberiotoxin (IBTX; 100 nM) and paxilline (Pax; 1 μM); or the BK channel activator NS1619 (10 μM) prior to assays. Whilst none of the tested compounds interfered with the mitochondrial activity of the cells (i.e. did not have adverse effects on general cell physiology; Fig. 5A), both IBTX and Pax significantly reduced the proliferation rate in CPCs (to 61.8%, $P < 0.001$; and 62.1%, $P = 0.002$, respectively), but had no significant effect in MSCs (Fig. 5B).

4. *Electrophysiological properties of chondroprogenitor cells*

CPC and MSC cell lines with a characteristic mesenchymal morphology were grown under standard culturing conditions prior to preparation for DEP analysis (Fig. 6A). The measured DEP spectra of the cell lines were used to determine specific membrane capacitance (C_{spec}) and conductance (G_{spec}) values; as these calculations take cell size into account (the values of capacitance and conductance are cell size independent), the cell radii were determined after trypsinisation, which were statistically different (11.00 ± 1.37 μm for MSC and 9.67 ± 1.43 for CPC; $P < 0.001$). The electrophysiological properties of CPC and MSC cells are shown in Fig. 6B, and summarised in Table 6. Effective membrane capacitance (C_{Eff}) is a measure of the ability of the membrane to store charge and generate a dipole in a frequency-dependent manner in DEP. The C_{Eff} values of CPC and MSC cells were not significantly different from each other (12.84 ± 4.44 mF m^{-2} vs. 11.29 ± 3.71 mF m^{-2} for CPC and MSC, respectively; $P = 0.298$). The membrane capacitance per cell area values were also very similar between CPC and MSC (14.86 ± 5.13 pF and 17.16 ± 5.65 pF; $P = 0.230$). The intracellular conductivities of CPC and MSC were 0.19 ± 0.06 S m^{-1} and 0.22 ± 0.06 S m^{-1} ($P = 0.202$), respectively. The greatest difference between the two cells was seen with regards to the specific membrane conductance (G_{spec}) parameter: CPCs were characterised by a significantly higher G_{Spec} value (827.43 ± 215.6 S m^{-2}) than MSCs (623.15 ± 45.05 S m^{-2}; $P = 0.006$), which showed a 32.79% difference. Representative DEP spectra for CPC and MSC cells are shown in Fig. 6C.

As RT-pPCR analysis revealed changes in the expression of several ion channels at the mRNA level, whole cell currents were examined. Both CPC and MSC cells were heterogeneous in respect to ionic current expression. Significant current was recorded in 3 out of 8 CPC cells. The voltage dependent features of these outward currents were reminiscent of that of BK channels. In addition, the time-dependent component was inhibited by Pax, indicating that the current was partially carried by BK channels. The linear component of the current was not specified further. In a similar way, Pax sensitive composite current was observed in 2 out of 4 MSC cells (Figure 7A–B). The resting membrane potential of CPCs did not differ significantly from that of MSCs as determined by whole-cell patch clamp measurements (–24.1 mV vs. –21.3 mV; $P = 0.63$) (Figure 7C).

Discussion

OA is a multi-faceted and highly heterogenous whole-joint disease without a common pathophysiological pathway. Therefore, it is unlikely that a single therapeutic target can halt or reverse the course of disease progression. There are currently no therapeutic strategies able to halt or significantly delay OA progression. The existing pharmacological treatments are also unable to sustain effective and long-lasting symptomatic relief. At present, joint replacement with an artificial prosthesis is the single most effective measure to improve patient quality of life, but of course not all OA patients will progress to this stage (Conaghan, Cook, Hamilton, & Tak, 2019). To develop novel therapeutic approaches targeting OA, a more profound understanding of the molecular mechanisms of the disease is required. A broad spectrum of ongoing trials and treatment options target various aspects of the disease, including cartilage and bone regeneration or repair, inflammatory and pain processes, altered metabolic pathways, and senescence (Grassel & Muschter, 2020).

Certain stem cell-based cartilage regenerative approaches are already in phase I clinical study stage. BM-MSCs and adipose tissue-derived MSCs (AD-MSCs) are currently the preferred cell types for regenerative strategies (Grassel & Muschter, 2020). However, whether MSCs are really the optimal cell population for cartilage regenerative therapy is still controversial. In this study, we turned our attention to alternative cell sources with potentially superior chondrogenic potential compared to BM-MSCs, which could be exploited for future cartilage regenerative therapies. Migratory CPCs have been partially characterised; they are known to exhibit a distinct transcriptomic signature compared to osteoblasts, chondrocytes and immortalised foetal chondrocytes (T/C-28 cells) (Koelling et al., 2009). However, the specific cellular identity and detailed molecular phenotype of CPCs is still elusive. Therefore, the aim of this study was to elucidate the biology and phenotype of CPCs by comparing their transcriptomic profile with BM-MSCs. Given the unique ionic composition of the CPC niche within the ECM of diseased cartilage, we were especially interested in differences in the channelome of CPCs, which may potentially harbour transporters responsible for maintaining the progenitor phenotype under inflammatory conditions. We also mapped the electrophysiological profile of CPCs using patch-clamp and DEP.

We have recently analysed the surfaceome of CPCs using selective cell surface protein labelling followed by high-throughput mass spectrometry and identified alterations in the composition of the surfaceome

compared to BM-MSCs (Matta et al., 2019). However, even the high-throughput mass spectrometry-based approach that we employed was not sensitive enough to detect alterations in very low-abundance ion channels and transporters. Here, we performed microarray analysis and compared the global gene expression signatures of CPCs to BM-MSCs. CPCs harboured a distinct transcriptomic profile and mRNA expression pattern that was different to that of MSCs. Pathway analysis confirmed that mainly cell cycle-related and DNA/nucleic acid metabolism related GO categories were overrepresented in the list of genes with significantly different expression levels. There was a 64% correlation with the direction of fold changes of differentially expressed transporter genes when we compared their pattern to the data generated by quantitative mass spectrometric analysis on the surfaceome of CPC and MSC cells (Table S3 in the Supporting information; see also Supplementary file 2) (Matta et al., 2019).

Differential transporter gene expression profiles

We chose to study the profiles of those ion channel and transporter families that are may have a relevance in chondroprogenitor cell physiology (Barrett-Jolley et al., 2010; Matta & Zakany, 2013; Mobasheri et al., 2019). The most widely reported ion channels in both chondrocytes and MSCs are potassium channels (Mobasheri et al., 2012; Pchelintseva & Djamgoz, 2018). The human genome contains around 70 different potassium channel genes, which makes them the largest family of membrane ion channels (Mobasheri et al., 2012). The α-subunit (*KCNMA1*) of the large conductance Ca^{2+}-activated potassium channel (BK, MaxiK), as well as the intermediate Ca^{2+}-activated potassium channel (IK, KCNN4, SK4, $K_{Ca}3.1$) transcripts displayed the largest fold changes, with a 50% upregulation in CPCs. BK channels have been detected in undifferentiated MSCs both at the mRNA level and by single channel recordings (Kawano, Otsu, Shoji, Yamagata, & Hiraoka, 2003), and also in mature chondrocytes (Mobasheri et al., 2010). MaxiK channels may play various roles in chondrocytes including volume regulation, oxygen sensing, and mechanotransduction (Mobasheri et al., 2012). Since BK channels have been implicated in driving MSC differentiation (Pchelintseva & Djamgoz, 2018), perhaps the fact that CPCs are more committed to the chondrogenic lineage than undifferentiated MSCs may explain the higher levels of *KCNMA1* both at the transcript and at the protein level (Matta et al., 2019). In addition, BK channel function was reported to modulate $[Ca^{2+}]_i$ oscillations in various cell types (Mizutani et al., 2016; Wakle-Prabagaran et al., 2016). Since we previously detected periodic fluctuations in resting cytosolic Ca^{2+} levels in CPCs (Matta et al., 2015), MaxiK channels may also play a central role in setting the RMP and modulating cell volume following the activation of purinergic signalling in CPCs. BK channels may also be potential drug targets to protect against joint degeneration in OA (Haidar et al., 2020). In an *in vitro* model of synovial inflammation, *KCNMA1* was found to be upregulated following cytokine treatment in primary synovial fibroblasts (Haidar et al., 2020). BK channel expression was also found to be upregulated in human OA cartilage (Lewis et al., 2013). Given that the migratory CPCs used in this study had been isolated from late-stage OA, the increased *KCNMA1* expression may also be a result of their original inflammatory niche. Since BK channels are known to regulate proliferation in BM-MSCs (Zhang et

al., 2014), it is not surprising that Pax has significantly lowered this parameter, especially in CPCs. The increased abundance of *KCNN4* transcripts in CPCs may reflect their inherently enhanced cell motility as IK channels have a confirmed role in migration (Pchelintseva & Djamgoz, 2018).

As far as other differentially expressed potassium channels are concerned, *KCNB1* (Kv2.1), *KCND2* (Kv4.2) and *KCNH6* (Kv11.2, HERG-2) were expressed at lower abundance in CPCs. The proteins encoded by these genes are responsible for outward or inward K^+ currents and are involved in regulating RMP. Whilst Kv2.1 was detected at low levels in MSCs, Kv4.2 is an abundantly expressed K^+ channel isoform (Heubach et al., 2004; G. R. Li, Sun, Deng, & Lau, 2005; Pillozzi & Becchetti, 2012).

Voltage-gated sodium channels are responsible for action potential initiation and propagation in excitable cells, and they are also expressed at low levels in non-excitable cells including chondrocytes (Barrett-Jolley et al., 2010), where their potential physiological roles could be varied (Abdul Kadir, Stacey, & Barrett-Jolley, 2018). Na^+ is the most abundant cation in cartilage ECM, yet not much is known about sodium channels and their role in chondrocyte homeostasis or chondrogenesis. The sodium channel which is implicated in MSCs is Nav1.5 (encoded by *SCN5A*) (G. R. Li et al., 2005), but that channel was not found to be differentially expressed in CPCs and MSCs. Of the voltage-gated sodium channels, *SCN2A* (coding for Nav1.2) was upregulated in CPCs; in contrast, *SCNN1D* (coding for the epithelial non voltage-gated sodium channel ENaCD) was less abundant in CPCs. ENaCs are expressed in chondrocytes (Shakibaei & Mobasheri, 2003; Trujillo et al., 1999) and have been implicated in mediating mechanotransduction in chondrocytes as well as osteoblasts (Mobasheri, Barrett-Jolley, Shakibaei, Canessa, & Martin-Vasallo, 2005; Mobasheri & Martin-Vasallo, 1999). They also participate in volume regulatory processes in mature chondrocytes (Lewis et al., 2013). Closely related to ENaC, *ASIC1*, the gene encoding the acid-sensing ion channel 1, was downregulated in CPCs. ASIC are extracellular H^+-activated ligand-gated cation channels, which play critical roles in physiological and pathological conditions (Zhou et al., 2016). *ASIC1* mediates pyroptosis in chondrocytes in response to extracellular acidosis, which is one of the important micro-environmental changes and key pathogenic features in degenerative joint disorders (Wu, Ren, Zhou, Ge, & Chen, 2019).

Calcium plays central roles in cell physiology in non-excitable cells such as chondrocytes (Suzuki et al., 2020). Dynamic changes in calcium signalling has been shown to be paramount to chondrogenesis (Matta & Zakany, 2013), and we have described earlier the calcium homeostasis of CPCs (Matta et al., 2015). Store-operated Ca^{2+} entry (SOCE), one of the main sources of Ca^{2+} influx, is mediated by Ca^{2+} release-activated Ca^{2+} channels (CRAC) formed of ORAI1, ORAI2 and ORAI3 proteins. Whilst the importance of ORAI1 for SOCE is well established, that of ORAI2 and ORAI3 remains elusive. We found that ORAI2 was present in lower abundance in CPCs; ORAI2 has been reported to modulate the magnitude of SOCE (Inayama et al., 2015; Vaeth et al., 2017), which further pinpoints the important role of SOCE in CPC homeostasis. Given that purinergic signalling regulates intracellular Ca^{2+} oscillations in CPCs and MSCs (Jiang, Mousawi, Yang, & Roger, 2017; Matta et al., 2015), we also looked at differences in purinergic receptor transcript levels. The only gene with a significantly altered expression was *P2RY2*,

which codes for a metabotropic receptor involved in the negative regulation of the osteogenic differentiation of BM-MSCs (W. Li et al., 2016). Transient receptor potential (TRP) channels are non-selective plasma membrane cation channels with a known role in mediating chondrogenesis (Parate et al., 2017; Somogyi et al., 2015). *TRPC4* and *TRPV2* were present at lower abundance in CPCs; however, none of these channels are widely discussed in the context of cartilage regeneration.

Electrophysiological profiling of CPCs

Having established the channelome of CPCs at the transcript level, we then looked at whether the global electrophysiological profile (electrome) of the progenitor cells was different from that of BM-MSCs. In addition to conventional patch clamping, we also employed DEP, which has been shown to be an efficient quantitative method of differentiating between closely related cell types e.g. in the bone marrow (Ismail, Hughes, Mulhall, Oreffo, & Labeed, 2015). DEP can be used for both assessing the passive electrical properties of cellular components, and as the basis for a separation method (Mahabadi, Labeed, & Hughes, 2018). This could be especially relevant for CPCs present at very low abundance in arthritic cartilage, given that a truly reliable cell surface marker has still not been identified. Inherent cell properties that do not require the use of specific labelling for detection would provide a unique means to identify progenitors biased to particular differentiated cell fates. Whilst the effective membrane capacitance and the intracellular conductivity values did not differ, we report membrane conductance as a specific electrophysiological property that reflects the differentiation stage of human CPCs and MSCs. Membrane conductivity is a parameter that describes the potential of the membrane to transmit charge; and is indicative of ionic flux (Henslee et al., 2017).

We employed patch clamping to establish the RMP of CPCs, which was not statistically different from that of MSCs. The V_m value of MSCs detected in our study (approx. –20 mV) was similar to what has been observed earlier (–10 mV) (Kawano et al., 2003). The RMP of mature chondrocytes is dependent on non-selective cation channels (Lewis et al., 2011), the majority of which did not show statistically different expression between MSCs and CPCs, which probably explains why there is no difference in RMP as observed in this study. As described above, various K^+ channels were observed at the transcript level in both cell types; therefore, we studied the outward whole cell currents in CPC and MSC cells. Both cell populations were heterogeneous with respect to ion current expression. Here we have provided evidence, for the first time, that MaxiK channels were functional in undifferentiated CPCs, as the voltage dependent features of the detected potassium currents were reminiscent of that of BK channels. In addition, the time-dependent component was inhibited by paxilline, indicating that the current was partially carried by BK channels. In line with our previous paper describing the Ca^{2+} homeostasis of CPCs (Matta et al., 2015), periodic increases in $[Ca^{2+}]_i$ may activate BK channels, and the ionic fluxes mediated by these channels may alter the RMP, which in turn modulates Ca^{2+} influx. Such a feedback loop has been recently proposed to exist in chondrocytes (Suzuki et al., 2020); we have now identified the key components of that loop in CPCs in this work.

Conclusions

A recent systematic review has analysed the outcome of 17 studies assessing articular cartilage repair after the clinical application of cell populations containing MSCs in human subjects with knee osteoarthritis (Ha, Park, Kim, & Lee, 2019). Significantly better clinical outcomes (improvement of the cartilage state on magnetic resonance imaging or repaired tissue on second-look arthroscopy) were reported in the MSC group in most of the studies. However, there is limited evidence to support the efficacy of intra-articular MSC-based therapy. This highlights opportunities for identifying alternative cell sources. Whilst the preferred cells used were bone, adipose tissue or umbilical cord-derived mesenchymal stem cells, perhaps exploiting the resident cartilage progenitor cell population present in both healthy and OA cartilage may further enhance the efficacy of such novel therapies. We demonstrate here that CPCs are a distinct cell population but are still similar to BM-MSCs in many ways. This work adds key mechanistic and cellular phenotype data to the in-depth characterisation of cartilage progenitor cells; however, further research is necessary to reconstruct the progenitor niche which would promote their hyaline cartilage regenerative potential.

Declarations

Supplementary Materials

The following supplementary materials are published online alongside the manuscript. Supplementary File 1 (PDF): Tables S1, S2 and S3; Figure S1.
Supplementary File 2 (XLSX): Correlation analysis between surfaceome proteins and their genes.

Acknowledgements

The authors are thankful to Mrs Krisztina Biróné Barna for skilful technical assistance. We would also like to acknowledge the contribution of Dr William Kothalawala Jayasekara.

Funding

CM was supported by the European Commission through a Marie Skłodowska-Curie Intra-European Fellowship for career development (project number: 625746; acronym: CHONDRION; FP7-PEOPLE-2013-IEF), the Premium Postdoctoral Research Fellowship of the Hungarian Academy of Sciences, and the Young Researcher Excellence Programme (grant number: FK-134304) of the National Research, Development and Innovation Office, Hungary. The research was co-financed by the Thematic Excellence Programme of the Ministry for Innovation and Technology in Hungary, within the framework of the Space Sciences thematic programme of the University of Debrecen (ED 18-1-2019-0028). AM was the co-ordinator of the D-BOARD Consortium funded by European Commission Framework 7 programme (EU

FP7; HEALTH.2012.2.4.5-2, project number 305815, Novel Diagnostics and Biomarkers for Early Identification of Chronic Inflammatory Joint Diseases). AM has received funding from the Deanship of Scientific Research (DSR), King AbdulAziz University (grant no. 1-141/1434 HiCi). AM is a member of the Arthritis Research UK Centre for Sport, Exercise, and Osteoarthritis, funded by Arthritis Research UK (Grant Reference Number: 20194). AM wishes to acknowledge financial support from the European Structural and Social Funds (ES Struktūrinės Paramos) through the Research Council of Lithuania (Lietuvos Mokslo Taryba) according to the activity 'Improvement of researchers' qualification by implementing world-class R&D projects' of Measure No. 09.3.3-LMT-K-712 (grant application code: 09.3.3-LMT-K-712-01-0157, agreement No. DOTSUT-215) and the new funding programme: Attracting Foreign Researchers for Research Implementation (2018-2022), Grant No 01.2.2-LMT-K-718-02-0022.

Availability of Data and Material

The data set is published in a MIAME compliant format in the GEO database (http://www.ncbi.nlm.nih.gov/geo/); accession numbers: GSM4885525-GSM4485530. All other data generated or analysed during this study are included in this published article [and its supplementary information files].

Author Contributions

Conceptualization, C.M. and A.M.; Methodology, C.M., R.L., C.F., J.A., S.M., M.P.H., A.M.; Software, M.C.U., S.P., F.L., M.P.H.; Validation, C.M., C.F., S.P.; Formal Analysis, C.M., R.L., C.F., E.H., J.A., F.L.; Investigation, C.M., R.L., C.F., G.D., M.C.U., S.P., E.H.; Resources, J.A., S.M., J.D., N.M., R.B.J., M.P.H., A.M.; Data Curation, C.M., R.L., C.F., J.A., M.C.U., E.H.; Writing – Original Draft Preparation, C.M., R.L.; Writing – Review & Editing, all authors; Visualization, C.M., M.C.U., G.D., S.P., E.H.; Supervision, N.M., R.B.J., F.L., J.D., S.M., A.M.; Project Administration, C.M., A.M.; Funding Acquisition, C.M., A.M.

Conflicts of Interest

The authors declare that they have no competing interests. This paper was written by the authors within the scope of their academic and research positions. None of the authors have any relationships that could be construed as biased or inappropriate. The funding bodies were not involved in the study design, data collection, analysis and interpretation. The decision to submit the paper for publication was not influenced by any the funding bodies.

References

Abdul Kadir, L., Stacey, M., & Barrett-Jolley, R. (2018). Emerging Roles of the Membrane Potential: Action Beyond the Action Potential. *Front Physiol, 9*, 1661. doi:10.3389/fphys.2018.01661

Al Maini, M., Al Weshahi, Y., Foster, H. E., Chehade, M. J., Gabriel, S. E., Saleh, J. A., . . . Woolf, A. D. (2020). A global perspective on the challenges and opportunities in learning about rheumatic and musculoskeletal diseases in undergraduate medical education : White paper by the World Forum on Rheumatic and Musculoskeletal Diseases (WFRMD). *Clin Rheumatol, 39*(3), 627-642. doi:10.1007/s10067-019-04544-y

Almassy, J., & Begenisich, T. (2012). The LRRC26 protein selectively alters the efficacy of BK channel activators. *Mol Pharmacol, 81*(1), 21-30. doi:10.1124/mol.111.075234

Andersen, C. L., Jensen, J. L., & Orntoft, T. F. (2004). Normalization of real-time quantitative reverse transcription-PCR data: a model-based variance estimation approach to identify genes suited for normalization, applied to bladder and colon cancer data sets. *Cancer Res, 64*(15), 5245-5250. doi:10.1158/0008-5472.CAN-04-0496

Archer, C. W., & Francis-West, P. (2003). The chondrocyte. *Int J Biochem Cell Biol, 35*(4), 401-404. doi:10.1016/s1357-2725(02)00301-1

Asmar, A., Barrett-Jolley, R., Werner, A., Kelly, R., Jr., & Stacey, M. (2016). Membrane channel gene expression in human costal and articular chondrocytes. *Organogenesis, 12*(2), 94-107. doi:10.1080/15476278.2016.1181238

Barrett-Jolley, R., Lewis, R., Fallman, R., & Mobasheri, A. (2010). The emerging chondrocyte channelome. *Front Physiol, 1*, 135. doi:10.3389/fphys.2010.00135

Barry, P. H., & Lynch, J. W. (1991). Liquid junction potentials and small cell effects in patch-clamp analysis. *J Membr Biol, 121*(2), 101-117. doi:10.1007/BF01870526

Broche, L. M., Labeed, F. H., & Hughes, M. P. (2005). Extraction of dielectric properties of multiple populations from dielectrophoretic collection spectrum data. *Phys Med Biol, 50*(10), 2267-2274. doi:10.1088/0031-9155/50/10/006

Buckwalter, J. A., Mankin, H. J., & Grodzinsky, A. J. (2005). Articular cartilage and osteoarthritis. *Instr Course Lect, 54*, 465-480. Retrieved from https://www.ncbi.nlm.nih.gov/pubmed/15952258

Conaghan, P. G., Cook, A. D., Hamilton, J. A., & Tak, P. P. (2019). Therapeutic options for targeting inflammatory osteoarthritis pain. *Nat Rev Rheumatol, 15*(6), 355-363. doi:10.1038/s41584-019-0221-y

De Loof, A. (2016). The cell's self-generated "electrome": The biophysical essence of the immaterial dimension of Life? *Commun Integr Biol, 9*(5), e1197446. doi:10.1080/19420889.2016.1197446

Dowthwaite, G. P., Bishop, J. C., Redman, S. N., Khan, I. M., Rooney, P., Evans, D. J., . . . Archer, C. W. (2004). The surface of articular cartilage contains a progenitor cell population. *J Cell Sci, 117*(Pt 6), 889-897. doi:10.1242/jcs.00912

Fellows, C. R., Williams, R., Davies, I. R., Gohil, K., Baird, D. M., Fairclough, J., . . . Khan, I. M. (2017). Characterisation of a divergent progenitor cell sub-populations in human osteoarthritic cartilage: the role of telomere erosion and replicative senescence. *Sci Rep, 7*, 41421. doi:10.1038/srep41421

Gomoll, A. H., & Minas, T. (2014). The quality of healing: articular cartilage. *Wound Repair Regen, 22 Suppl 1*, 30-38. doi:10.1111/wrr.12166

Grassel, S., & Muschter, D. (2020). Recent advances in the treatment of osteoarthritis. *F1000Res, 9*. doi:10.12688/f1000research.22115.1

Ha, C. W., Park, Y. B., Kim, S. H., & Lee, H. J. (2019). Intra-articular Mesenchymal Stem Cells in Osteoarthritis of the Knee: A Systematic Review of Clinical Outcomes and Evidence of Cartilage Repair. *Arthroscopy, 35*(1), 277-288 e272. doi:10.1016/j.arthro.2018.07.028

Haidar, O., O'Neill, N., Staunton, C. A., Bavan, S., O'Brien, F., Zouggari, S., . . . Barrett-Jolley, R. (2020). Pro-inflammatory Cytokines Drive Deregulation of Potassium Channel Expression in Primary Synovial Fibroblasts. *Front Physiol, 11*, 226. doi:10.3389/fphys.2020.00226

Hdud, I. M., Mobasheri, A., & Loughna, P. T. (2014). Effect of osmotic stress on the expression of TRPV4 and BKCa channels and possible interaction with ERK1/2 and p38 in cultured equine chondrocytes. *Am J Physiol Cell Physiol, 306*(11), C1050-1057. doi:10.1152/ajpcell.00287.2013

Henrotin, Y., Sanchez, C., Bay-Jensen, A. C., & Mobasheri, A. (2016). Osteoarthritis biomarkers derived from cartilage extracellular matrix: Current status and future perspectives. *Ann Phys Rehabil Med, 59*(3), 145-148. doi:10.1016/j.rehab.2016.03.004

Henslee, E. A., Crosby, P., Kitcatt, S. J., Parry, J. S. W., Bernardini, A., Abdallat, R. G., . . . Labeed, F. H. (2017). Rhythmic potassium transport regulates the circadian clock in human red blood cells. *Nat Commun, 8*(1), 1978. doi:10.1038/s41467-017-02161-4

Heubach, J. F., Graf, E. M., Leutheuser, J., Bock, M., Balana, B., Zahanich, I., . . . Ravens, U. (2004). Electrophysiological properties of human mesenchymal stem cells. *J Physiol, 554*(Pt 3), 659-672. doi:10.1113/jphysiol.2003.055806

Hoettges, K. F., Henslee, E. A., Torcal Serrano, R. M., Jabr, R. I., Abdallat, R. G., Beale, A. D., . . . Hughes, M. P. (2019). Ten-Second Electrophysiology: Evaluation of the 3DEP Platform for high-speed, high-accuracy cell analysis. *Sci Rep, 9*(1), 19153. doi:10.1038/s41598-019-55579-9

Hoettges, K. F., Hubner, Y., Broche, L. M., Ogin, S. L., Kass, G. E., & Hughes, M. P. (2008). Dielectrophoresis-activated multiwell plate for label-free high-throughput drug assessment. *Anal Chem, 80*(6), 2063-2068.

doi:10.1021/ac702083g

Hunter, D. J., & Bierma-Zeinstra, S. (2019). Osteoarthritis. *Lancet, 393*(10182), 1745-1759. doi:10.1016/S0140-6736(19)30417-9

Inayama, M., Suzuki, Y., Yamada, S., Kurita, T., Yamamura, H., Ohya, S., . . . Imaizumi, Y. (2015). Orai1-Orai2 complex is involved in store-operated calcium entry in chondrocyte cell lines. *Cell Calcium, 57*(5-6), 337-347. doi:10.1016/j.ceca.2015.02.005

Ismail, A., Hughes, M. P., Mulhall, H. J., Oreffo, R. O., & Labeed, F. H. (2015). Characterization of human skeletal stem and bone cell populations using dielectrophoresis. *J Tissue Eng Regen Med, 9*(2), 162-168. doi:10.1002/term.1629

Jiang, L. H., Mousawi, F., Yang, X., & Roger, S. (2017). ATP-induced Ca(2+)-signalling mechanisms in the regulation of mesenchymal stem cell migration. *Cell Mol Life Sci, 74*(20), 3697-3710. doi:10.1007/s00018-017-2545-6

Kawano, S., Otsu, K., Shoji, S., Yamagata, K., & Hiraoka, M. (2003). Ca(2+) oscillations regulated by Na(+)-Ca(2+) exchanger and plasma membrane Ca(2+) pump induce fluctuations of membrane currents and potentials in human mesenchymal stem cells. *Cell Calcium, 34*(2), 145-156. doi:10.1016/s0143-4160(03)00069-1

Koelling, S., Kruegel, J., Irmer, M., Path, J. R., Sadowski, B., Miro, X., & Miosge, N. (2009). Migratory chondrogenic progenitor cells from repair tissue during the later stages of human osteoarthritis. *Cell Stem Cell, 4*(4), 324-335. doi:10.1016/j.stem.2009.01.015

Labeed, F. H., Lu, J., Mulhall, H. J., Marchenko, S. A., Hoettges, K. F., Estrada, L. C., . . . Flanagan, L. A. (2011). Biophysical characteristics reveal neural stem cell differentiation potential. *PLoS One, 6*(9), e25458. doi:10.1371/journal.pone.0025458

Lewis, R., Asplin, K. E., Bruce, G., Dart, C., Mobasheri, A., & Barrett-Jolley, R. (2011). The role of the membrane potential in chondrocyte volume regulation. *J Cell Physiol, 226*(11), 2979-2986. doi:10.1002/jcp.22646

Lewis, R., & Barrett-Jolley, R. (2015). Changes in Membrane Receptors and Ion Channels as Potential Biomarkers for Osteoarthritis. *Front Physiol, 6*, 357. doi:10.3389/fphys.2015.00357

Lewis, R., Feetham, C. H., Gentles, L., Penny, J., Tregilgas, L., Tohami, W., . . . Barrett-Jolley, R. (2013). Benzamil sensitive ion channels contribute to volume regulation in canine chondrocytes. *Br J Pharmacol, 168*(7), 1584-1596. doi:10.1111/j.1476-5381.2012.02185.x

Li, G. R., Sun, H., Deng, X., & Lau, C. P. (2005). Characterization of ionic currents in human mesenchymal stem cells from bone marrow. *Stem Cells, 23*(3), 371-382. doi:10.1634/stemcells.2004-0213

Li, W., Wei, S., Liu, C., Song, M., Wu, H., & Yang, Y. (2016). Regulation of the osteogenic and adipogenic differentiation of bone marrow-derived stromal cells by extracellular uridine triphosphate: The role of P2Y2 receptor and ERK1/2 signaling. *Int J Mol Med, 37*(1), 63-73. doi:10.3892/ijmm.2015.2400

Loeser, R. F., Goldring, S. R., Scanzello, C. R., & Goldring, M. B. (2012). Osteoarthritis: a disease of the joint as an organ. *Arthritis Rheum, 64*(6), 1697-1707. doi:10.1002/art.34453

Mahabadi, S., Labeed, F. H., & Hughes, M. P. (2018). Dielectrophoretic analysis of treated cancer cells for rapid assessment of treatment efficacy. *Electrophoresis, 39*(8), 1104-1110. doi:10.1002/elps.201700488

Maleckar, M. M., Martin-Vasallo, P., Giles, W. R., & Mobasheri, A. (2020). Physiological Effects of the Electrogenic Current Generated by the Na+/K+ Pump in Mammalian Articular Chondrocytes. *Bioelectricity*, 258-268. doi:10.1089/bioe.2020.0036

Mankin, H. J., & Lippiello, L. (1970). Biochemical and metabolic abnormalities in articular cartilage from osteo-arthritic human hips. *J Bone Joint Surg Am, 52*(3), 424-434. Retrieved from https://www.ncbi.nlm.nih.gov/pubmed/4246573

Matta, C., Boocock, D. J., Fellows, C. R., Miosge, N., Dixon, J. E., Liddell, S., . . . Mobasheri, A. (2019). Molecular phenotyping of the surfaceome of migratory chondroprogenitors and mesenchymal stem cells using biotinylation, glycocapture and quantitative LC-MS/MS proteomic analysis. *Sci Rep, 9*(1), 9018. doi:10.1038/s41598-019-44957-y

Matta, C., Fodor, J., Miosge, N., Takacs, R., Juhasz, T., Rybaltovszki, H., . . . Zakany, R. (2015). Purinergic signalling is required for calcium oscillations in migratory chondrogenic progenitor cells. *Pflugers Arch, 467*(2), 429-442. doi:10.1007/s00424-014-1529-8

Matta, C., & Zakany, R. (2013). Calcium signalling in chondrogenesis: implications for cartilage repair. *Front Biosci (Schol Ed), 5*, 305-324. Retrieved from https://www.ncbi.nlm.nih.gov/pubmed/23277053

Mizutani, H., Yamamura, H., Muramatsu, M., Hagihara, Y., Suzuki, Y., & Imaizumi, Y. (2016). Modulation of Ca2+ oscillation and melatonin secretion by BKCa channel activity in rat pinealocytes. *Am J Physiol Cell Physiol, 310*(9), C740-747. doi:10.1152/ajpcell.00342.2015

Mobasheri, A., Barrett-Jolley, R., Shakibaei, M., Canessa, C. M., & Martin-Vasallo, P. (2005). Enigmatic Roles of the Epithelial Sodium Channel (ENaC) in Articular Chondrocytes and Osteoblasts: Mechanotransduction, Sodium Transport or Extracellular Sodium Sensing? In A. Kamkin & I. Kiseleva (Eds.), *Mechanosensitivity in Cells and Tissues*. Moscow.

Mobasheri, A., Lewis, R., Ferreira-Mendes, A., Rufino, A., Dart, C., & Barrett-Jolley, R. (2012). Potassium channels in articular chondrocytes. *Channels (Austin), 6*(6), 416-425. doi:10.4161/chan.22340

Mobasheri, A., Lewis, R., Maxwell, J. E., Hill, C., Womack, M., & Barrett-Jolley, R. (2010). Characterization of a stretch-activated potassium channel in chondrocytes. *J Cell Physiol, 223*(2), 511-518.

doi:10.1002/jcp.22075

Mobasheri, A., & Martin-Vasallo, P. (1999). Epithelial sodium channels in skeletal cells; a role in mechanotransduction? *Cell Biol Int, 23*(4), 237-240. doi:10.1006/cbir.1999.0405

Mobasheri, A., Matta, C., Uzieliene, I., Budd, E., Martin-Vasallo, P., & Bernotiene, E. (2019). The chondrocyte channelome: A narrative review. *Joint Bone Spine, 86*(1), 29-35. doi:10.1016/j.jbspin.2018.01.012

Mobasheri, A., Mobasheri, R., Francis, M. J., Trujillo, E., Alvarez de la Rosa, D., & Martin-Vasallo, P. (1998). Ion transport in chondrocytes: membrane transporters involved in intracellular ion homeostasis and the regulation of cell volume, free [Ca2+] and pH. *Histol Histopathol, 13*(3), 893-910. doi:10.14670/HH-13.893

Mow, V. C., Wang, C. C., & Hung, C. T. (1999). The extracellular matrix, interstitial fluid and ions as a mechanical signal transducer in articular cartilage. *Osteoarthritis Cartilage, 7*(1), 41-58. doi:10.1053/joca.1998.0161

Nakayama, N., Pothiawala, A., Lee, J. Y., Matthias, N., Umeda, K., Ang, B. K., . . . Sun, D. (2020). Human pluripotent stem cell-derived chondroprogenitors for cartilage tissue engineering. *Cell Mol Life Sci, 77*(13), 2543-2563. doi:10.1007/s00018-019-03445-2

Okamoto, T., Aoyama, T., Nakayama, T., Nakamata, T., Hosaka, T., Nishijo, K., . . . Toguchida, J. (2002). Clonal heterogeneity in differentiation potential of immortalized human mesenchymal stem cells. *Biochem Biophys Res Commun, 295*(2), 354-361. Retrieved from https://www.ncbi.nlm.nih.gov/pubmed/12150956

Parate, D., Franco-Obregon, A., Frohlich, J., Beyer, C., Abbas, A. A., Kamarul, T., . . . Yang, Z. (2017). Enhancement of mesenchymal stem cell chondrogenesis with short-term low intensity pulsed electromagnetic fields. *Sci Rep, 7*(1), 9421. doi:10.1038/s41598-017-09892-w

Pchelintseva, E., & Djamgoz, M. B. A. (2018). Mesenchymal stem cell differentiation: Control by calcium-activated potassium channels. *J Cell Physiol, 233*(5), 3755-3768. doi:10.1002/jcp.26120

Pillozzi, S., & Becchetti, A. (2012). Ion channels in hematopoietic and mesenchymal stem cells. *Stem Cells Int, 2012*, 217910. doi:10.1155/2012/217910

Saeed, A., Francini, N., White, L., Dixon, J., Gould, T., Rashidi, H., . . . Shakesheff, K. M. (2015). A thermoresponsive and magnetic colloid for 3D cell expansion and reconfiguration. *Adv Mater, 27*(4), 662-668. doi:10.1002/adma.201403626

Shakibaei, M., & Mobasheri, A. (2003). Beta1-integrins co-localize with Na, K-ATPase, epithelial sodium channels (ENaC) and voltage activated calcium channels (VACC) in mechanoreceptor complexes of mouse limb-bud chondrocytes. *Histol Histopathol, 18*(2), 343-351. doi:10.14670/HH-18.343

Somogyi, C. S., Matta, C., Foldvari, Z., Juhasz, T., Katona, E., Takacs, A. R., . . . Zakany, R. (2015). Polymodal Transient Receptor Potential Vanilloid (TRPV) Ion Channels in Chondrogenic Cells. *Int J Mol Sci, 16*(8), 18412-18438. doi:10.3390/ijms160818412

Suzuki, Y., Yamamura, H., Imaizumi, Y., Clark, R. B., & Giles, W. R. (2020). K(+) and Ca(2+) Channels Regulate Ca(2+) Signaling in Chondrocytes: An Illustrated Review. *Cells, 9*(7). doi:10.3390/cells9071577

Trujillo, E., Alvarez de la Rosa, D., Mobasheri, A., Gonzalez, T., Canessa, C. M., & Martin-Vasallo, P. (1999). Sodium transport systems in human chondrocytes. II. Expression of ENaC, Na+/K+/2Cl- cotransporter and Na+/H+ exchangers in healthy and arthritic chondrocytes. *Histol Histopathol, 14*(4), 1023-1031. doi:10.14670/HH-14.1023

Urban, J. P., Hall, A. C., & Gehl, K. A. (1993). Regulation of matrix synthesis rates by the ionic and osmotic environment of articular chondrocytes. *J Cell Physiol, 154*(2), 262-270. doi:10.1002/jcp.1041540208

Vaeth, M., Yang, J., Yamashita, M., Zee, I., Eckstein, M., Knosp, C., . . . Feske, S. (2017). ORAI2 modulates store-operated calcium entry and T cell-mediated immunity. *Nat Commun, 8*, 14714. doi:10.1038/ncomms14714

Wakle-Prabagaran, M., Lorca, R. A., Ma, X., Stamnes, S. J., Amazu, C., Hsiao, J. J., . . . England, S. K. (2016). BKCa channel regulates calcium oscillations induced by alpha-2-macroglobulin in human myometrial smooth muscle cells. *Proc Natl Acad Sci U S A, 113*(16), E2335-2344. doi:10.1073/pnas.1516863113

Wu, X., Ren, G., Zhou, R., Ge, J., & Chen, F. H. (2019). The role of Ca(2+) in acid-sensing ion channel 1a-mediated chondrocyte pyroptosis in rat adjuvant arthritis. *Lab Invest, 99*(4), 499-513. doi:10.1038/s41374-018-0135-3

Zhang, Y. Y., Yue, J., Che, H., Sun, H. Y., Tse, H. F., & Li, G. R. (2014). BKCa and hEag1 channels regulate cell proliferation and differentiation in human bone marrow-derived mesenchymal stem cells. *J Cell Physiol, 229*(2), 202-212. doi:10.1002/jcp.24435

Zhou, R. P., Wu, X. S., Wang, Z. S., Xie, Y. Y., Ge, J. F., & Chen, F. H. (2016). Novel Insights into Acid-Sensing Ion Channels: Implications for Degenerative Diseases. *Aging Dis, 7*(4), 491-501. doi:10.14336/AD.2015.1213

Tables

Gene Symbol	Fold-Change (CPC vs. MSC)	Rel. expression	*P*-value
Big conductance K channel			
KCNMA1	**1.674**	**CPC up vs MSC**	**0.016**
KCNMB1	1.119	No change	0.164
KCNMB2	1.029	No change	0.631
KCNMB3	-1.055	No change	0.536
KCNMB4	-1.050	CPC down vs MSC	0.024
Intermediate and small conductance K channels			
KCNN1	-1.158	No change	0.464
KCNN2	1.079	No change	0.452
KCNN3	-1.122	No change	0.132
KCNN4	**1.620**	**CPC up vs MSC**	**0.033**
Delayed rectifier K channels			
KCNA1	1.022	No change	0.782
KCNA2	1.065	No change	0.315
KCNA3	-1.001	No change	0.985
KCNA5	1.127	No change	0.079
KCNA6	-1.091	No change	0.384
KCNA7	1.123	No change	0.591
KCNA10	1.074	No change	0.217
KCNB1	**-1.210**	**CPC down vs MSC**	**0.048**
KCNA11	-1.053	No change	0.659
KCNA12	1.051	No change	0.476
KCNA13	-1.125	No change	0.109
KCNA14	-1.089	No change	0.529
KCNA15	-1.005	No change	0.940
KCNA16	1.041	No change	0.213
KCNA17	-1.055	No change	0.732
KCNA18	1.029	No change	0.826

A-type K channels			
KCNA4	1.118	No change	0.170
KCNC3	1.045	No change	0.750
KCNC4	1.034	No change	0.728
KCND1	-1.104	No change	0.480
KCND2	**-1.654**	**CPC down vs MSC**	**0.024**
KCND3	-1.173	No change	0.175
Outward rectifying K channel			
KCNH5	1.067	No change	0.123
Inward rectifying K channel			
KCNH2	-1.013	No change	0.873
KCNH6	**-1.166**	**CPC down vs MSC**	**0.037**
KCNH7	1.037	No change	0.786
Inward rectifying Kir channels			
KCNJ1	1.063	No change	0.485
KCNJ2	-1.262	No change	0.113
KCNJ3	1.077	No change	0.307
KCNJ4	1.078	No change	0.583
KCNJ5	1.032	No change	0.511
KCNJ6	-1.147	No change	0.143
KCNJ7	1.269	No change	0.161
KCNJ8	1.080	No change	0.370
KCNJ9	1.072	No change	0.144
KCNJ10	-1.050	No change	0.590
KCNJ11	1.005	No change	0.963
KCNJ12	1.012	No change	0.777
KCNJ13	1.154	No change	0.179
KCNJ14	1.160	No change	0.582
KCNJ15	1.075	No change	0.321

Slowly activating K channel			
KCNH3	1.010	No change	0.912
KCNH4	-1.066	No change	0.280
KCNH8	1.058	No change	0.277
Modifier/silencer K channels			
KCMF1	-1.233	No change	0.288
KCNG1	-1.057	No change	0.674
KCNG2	-1.191	No change	0.442
KCNG3	1.012	No change	0.880
KCNG4	-1.053	No change	0.413
KCNS1	-1.125	No change	0.243
KCNS2	1.191	No change	0.182
KCNS3	1.063	No change	0.390
KCNV1	1.104	No change	0.439
KCNV2	-1.037	No change	0.598
Other K channels			
KCNT1	-1.024	No change	0.597
KCNT2	-1.073	No change	0.614
KCNU1	1.070	No change	0.149

Table 1. Lists of genes coding for potassium ion channel (subunits), with fold change and significance (*P*-value) levels for each gene. Genes which were significantly up or down regulated in CPC *versus* MSC cells are highlighted in boldface; the red colour represents up regulation, and blue colour represent down regulation of expression.

Gene Symbol	Fold-Change (CPC vs. MSC)	Rel. expression	*P*-value
Voltage-gated sodium transporters			
SCN1A	1.029	No change	0.494
SCN2A	**1.310**	**CPC up vs MSC**	**0.027**
SCN3A	1.744	No change	0.257
SCN4A	1.022	No change	0.870
SCN5A	-1.140	No change	0.170
SCN7A	1.026	No change	0.487
SCN8A	1.057	No change	0.509
SCN9A	1.793	No change	0.181
SCN10A	-1.000	No change	0.997
SCN11A	-1.005	No change	0.950
Epithelial sodium channels			
SCNN1A	-1.047	No change	0.355
SCNN1B	-1.002	No change	0.977
SCNN1D	**-1.160**	**CPC down vs MSC**	**0.022**
SCNN1G	-1.018	No change	0.842

Table 2. Lists of genes coding for sodium ion channel (subunits), with fold change and significance (*P*-value) levels for each gene. Genes which were significantly up or down regulated in CPC *versus* MSC cells are highlighted in boldface; the red colour represents up regulation, and blue colour represent down regulation of expression.

Gene Symbol	Fold-Change (CPC vs. MSC)	Rel. expression	*P*-value
Calcium homeostasis			
SOCE			
ORAI1	-1.553	No change	0.168
ORAI2	**-1.462**	**CPC down vs MSC**	**0.008**
ORAI3	1.201	No change	0.673
STIM1	-1.182	No change	0.387
STIM2	-1.351	No change	0.093
Voltage-gated calcium channels. alpha subunit			
CACNA1A	1.040	No change	0.584
CACNA1B	1.055	No change	0.352
CACNA1D	1.005	No change	0.927
CACNA1E	1.009	No change	0.598
CACNA1F	1.088	No change	0.080
CACNA1G	-1.013	No change	0.849
CACNA1H	-1.087	No change	0.527
CACNA1I	1.017	No change	0.855
CACNA1S	-1.054	No change	0.419
Calcium release			
ITPR1	-1.195	No change	0.164
ITPR2	-1.423	No change	0.124
ITPR3	-1.015	No change	0.967
RYR1	1.001	No change	0.982
RYR2	1.003	No change	0.950
RYR3	1.010	No change	0.587
Calcium pumps and transporters			
ATP2A1	1.021	No change	0.701
ATP2A2	-1.424	No change	0.120
ATP2A3	**-1.458**	**CPC down vs MSC**	**0.048**

ATP2B1	-1.245	No change	0.374
ATP2B2	1.010	No change	0.898
ATP2B3	1.009	No change	0.879
ATP2B4	1.149	No change	0.345
SLC8A1	1.070	No change	0.220
SLC8A2	1.082	No change	0.335
SLC8A3	-1.008	No change	0.816
Metabotropic P2Y receptors			
P2RY1	1.063	No change	0.380
P2RY2	**-1.573**	**CPC down vs MSC**	**0.003**
P2RY4	1.090	No change	0.355
P2RY6	1.032	No change	0.723
P2RY8	1.054	No change	0.515
P2RY10	1.079	No change	0.519
P2RY12	1.018	No change	0.717
P2RY13	1.055	No change	0.203
P2RY14	1.073	No change	0.582
Non-selective cation channels			
P2X purinergic receptors			
P2RX1	-1.043	No change	0.548
P2RX2	-1.098	No change	0.170
P2RX3	-1.117	No change	0.385
P2RX4	-1.352	No change	0.083
P2RX5	1.039	No change	0.823
P2RX6	-1.033	No change	0.710
P2RX7	1.102	No change	0.296
Transient Receptor Potential Channels			
TRPC1	-1.174	No change	0.405

TRPC2	1.025	No change	0.551
TRPC3	-1.157	No change	0.127
TRPC4	**-1.642**	**CPC down vs MSC**	**0.008**
TRPC5	1.075	No change	0.270
TRPC6	-1.050	No change	0.129
TRPC7	-1.001	No change	0.979
TRPV1	-1.041	No change	0.739
TRPV2	**-1.792**	**CPC down vs MSC**	**0.015**
TRPV3	1.056	No change	0.478
TRPV4	1.137	No change	0.459
TRPV5	-1.066	No change	0.430
TRPV6	-1.013	No change	0.824

Table 3. Lists of genes coding for calcium and non-selective ion channel (subunits), with fold change and significance (*P*-value) levels for each gene. Genes which were significantly up or down regulated in CPC *versus* MSC cells are highlighted in boldface; the red colour represents up regulation, and blue colour represent down regulation of expression.

Gene Symbol	Fold-Change (CPC vs. MSC)	Rel. expression	*P*-value
Acid-sensitive cation channels			
ASIC1	**-1.289**	**CPC down vs MSC**	**0.005**
ASIC2	1.044	No change	0.829
ASIC3	1.060	No change	0.388
ASIC4	1.065	No change	0.354
Calcium activated chloride channels			
CLCA1	1.035	No change	0.619
CLCA2	-1.103	No change	0.236
CLCA3P	1.080	No change	0.162
CLCA4	1.013	No change	0.736
CLCN family			
CLCN1	-1.193	No change	0.150
CLCN2	1.067	No change	0.217
CLCN3	-1.081	No change	0.806
CLCN4	-1.077	No change	0.703
CLCN5	-1.121	No change	0.476
CLCNKA	-1.040	No change	0.657
CLCNKB	-1.263	No change	0.291
Intracellular chloride channels			
CLIC2	1.015	No change	0.853
CLIC3	1.182	No change	0.472
CLIC4	-1.153	No change	0.217
CLIC5	1.226	No change	0.177
CLIC6	1.114	No change	0.065

Table 4. Lists of genes coding for chloride and acid sensitive cation channel (subunits), with fold change and significance (*P*-value) levels for each gene. Genes which were significantly up or down regulated in

CPC *versus* MSC cells are highlighted in boldface; the red colour represents up regulation, and blue colour represent down regulation of expression.

Gene Symbol	Fold Change (CPC vs MSC)	Rel. expression	*P*-value
Reference gene			
PPIA	1.00		0.49
Voltage-gated calcium channel alpha subunit			
CACNA1A	-1.22		0.11
CACNA1B	-2.24		0.66
CACNA1D	**2.09**	**CPC up vs MSC**	**0.07**
CACNA1E	*N/A*		*N/A*
CACNA1F	*N/A*		*N/A*
CACNA1G	-1.26		0.48
CACNA1H	**MSC only**	**MSC only**	**N/A**
CACNA1I	*N/A*		*N/A*
CACNA1S	**MSC only**	**MSC only**	**N/A**
CACNA1C	-1.57		0.68
Metabotropic purinergic receptor			
P2RY1	**MSC only**	**MSC only**	**N/A**
P2RY2	4.33		0.02
P2RY4	-0.97		0.30
P2RY6	**1.50**	**CPC up vs MSC**	**0.05**
P2RY11	**MSC only**	**MSC only**	**N/A**
P2RY12	**1.62**	**CPC up vs MSC**	**0.05**
P2RY13	-2.42		0.66
P2RY14	*N/A*		*N/A*
Ionotropic purinergic receptor			
P2RX1	**-1.27**	**CPC down vs MSC**	**0.09**
P2RX2	*N/A*		*N/A*
P2RX3	**MSC only**	**MSC only**	**N/A**
P2RX4	1.09		0.31
P2RX5	1.98		0.13

P2RX6	**2.27**	**CPC up vs MSC**	**0.06**
P2RX7	-1.67		0.33
Transient receptor potential vanilloid			
TRPV1	-1.18		0.47
TRPV2	**38.94**	**CPC up vs MSC**	**0.01**
TRPV3	1.62		0.11
TRPV4	-1.51		0.47
TRPV5	*N/A*		*N/A*
TRPV6	*N/A*		*N/A*
Transient receptor potential canonical			
TRPC1	-1.09		0.24
TRPC3	**8.04**	**CPC up vs MSC**	**0.00**
TRPC4	**1.48**	**CPC up vs MSC**	**0.09**
TRPC5	*N/A*		*N/A*
TRPC6	1.51		0.05
Store-operated calcium entry (SOCE)			
ORAI1	1.37		0.27
ORAI2	1.55		0.33
ORAI3	-0.89		0.34
STIM1	-0.92		0.43
STIM2	**1.56**	**CPC up vs MSC**	**0.02**
Calcium release channel			
ITPR1	-1.14		0.45
ITPR2	-1.14		0.14
ITPR3	-1.77		0.57
RYR1	**MSC only**	**MSC only**	**N/A**
RYR2	*N/A*		*N/A*
RYR3	**MSC only**	**MSC only**	**N/A**
Calcium active transporter			

ATP2A1	**6.05**	**CPC up vs MSC**	**0.06**
ATP2A2	1.32		0.25
ATP2A3	**13.44**	**CPC up vs MSC**	**0.00**
ATP2B1	1.27		0.22
ATP2B2	**MSC only**	**MSC only**	**N/A**
ATP2B3	**MSC only**	**MSC only**	**N/A**
ATP2B4	-1.60		0.66
Sodium/calcium exchanger			
SLC8A1	**CPC only**	**CPC up vs MSC**	**N/A**
SLC8A2	-2.19		0.50
SLC8A3	**MSC only**	**CPC down vs MSC**	**N/A**
Sodium permeable non-voltage-sensitive ion channel			
SCNN1A	**1.28**	**CPC up vs MSC**	**0.02**
SCNN1B	*N/A*		*N/A*
SCNN1D	*N/A*		*N/A*
SCNN1G	*N/A*		*N/A*
Chloride channel			
CLCN1	*N/A*		*N/A*
CLCN2	-1.84		0.59
CLCN4	-1.32		0.58
CLCN5	1.35		0.31
CLCN6	1.29		0.27
CLCN7	1.38		0.31
CLCNKA	-6.11		0.28
CLCNKB	**MSC only**	**MSC only**	**N/A**
CLIC1	-0.99		0.26
CLIC3	-2.05		0.80
CLIC4	-0.88		0.26
CLIC5	**MSC only**	**MSC only**	**N/A**

CLIC6	-2.96		0.91
CLCA1	*N/A*		*N/A*
CLCA2	-1.77		0.63
CLCA3P	*N/A*		*N/A*
Calcium-activated potassium channel subunit			
KCNMA1	**1.95**	**CPC up vs MSC**	**0.04**
KCNMB1	**MSC only**	**MSC only**	**N/A**
KCNMB2	**MSC only**	**MSC only**	**N/A**
KCNMB3	**1.39**	**CPC up vs MSC**	**0.04**
KCNMB4	**25.82**	**CPC up vs MSC**	**0.01**
KCNN1	-1.01		0.12
KCNN2	*N/A*		*N/A*
KCNN3	**MSC only**	**MSC only**	**N/A**
KCNN4	-3.64		0.82

Table 5. Results of the qPCR array for selected genes. Table shows fold change and significance (*P*-value) levels for each gene. Transcripts which were significantly up or down regulated in CPC *versus* MSC cells are highlighted in boldface; the red colour represents up regulation, and blue colour represent down regulation of expression.

	CPC	*MSC*	*P-value*
Cell radius (μm)	9.6 (± 1.43)	11 (± 1.37)	0.000
Effective membrane capacitance (mF/m^2)	12.84 (± 4.44)	11.29 (± 3.71)	0.298
Membrane capacitance per cell (pF)	14.86 (± 5.13)	17.16 (± 5.65)	0.231
Intracellular conductivity (S/m)	0.19 (± 0.06)	0.22 (± 0.06)	0.203
Specific membrane conductance (S/m^2)	827.48 (± 215.64)	623.15 (± 168.56)	0.006

Table 6. Electrophysiological characteristics of CPC and MSC cells grown in standard monolayer cultures as determined by the DEP well chip and the single-shell model applied to the data. Values shown were averaged over 3 repeats of separate populations with ± SD given in brackets.

Figures

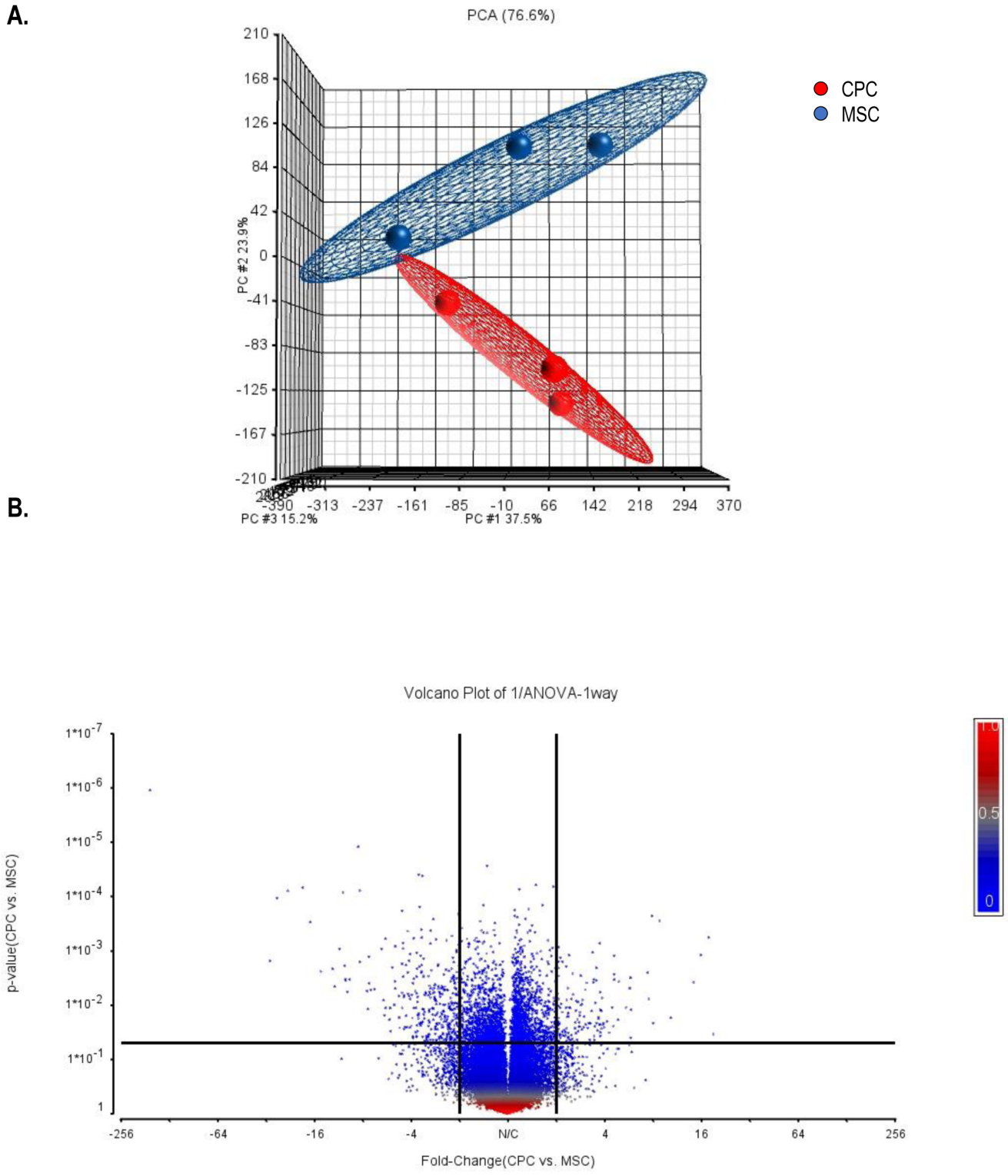

Figure 1

(A) Principal component analysis (PCA) showing transcriptomic differences between expression microarray data of both CPC and MSC cells. Each sample group is represented by a sphere and is colour-coded to indicate the corresponding cell type category. There is a clear difference in the transcriptomic clustering between MSC and CPC samples. (B) Volcano plot showing fold-change and p-value for the comparison of CPC versus MSC cells. The vertical lines correspond to 2-fold up and down-regulation,

respectively, and the horizontal line represent a P-value of < 0.05. Based on these parameters, the dots in the upper left and right quadrants represent differentially expressed genes with statistical significance.

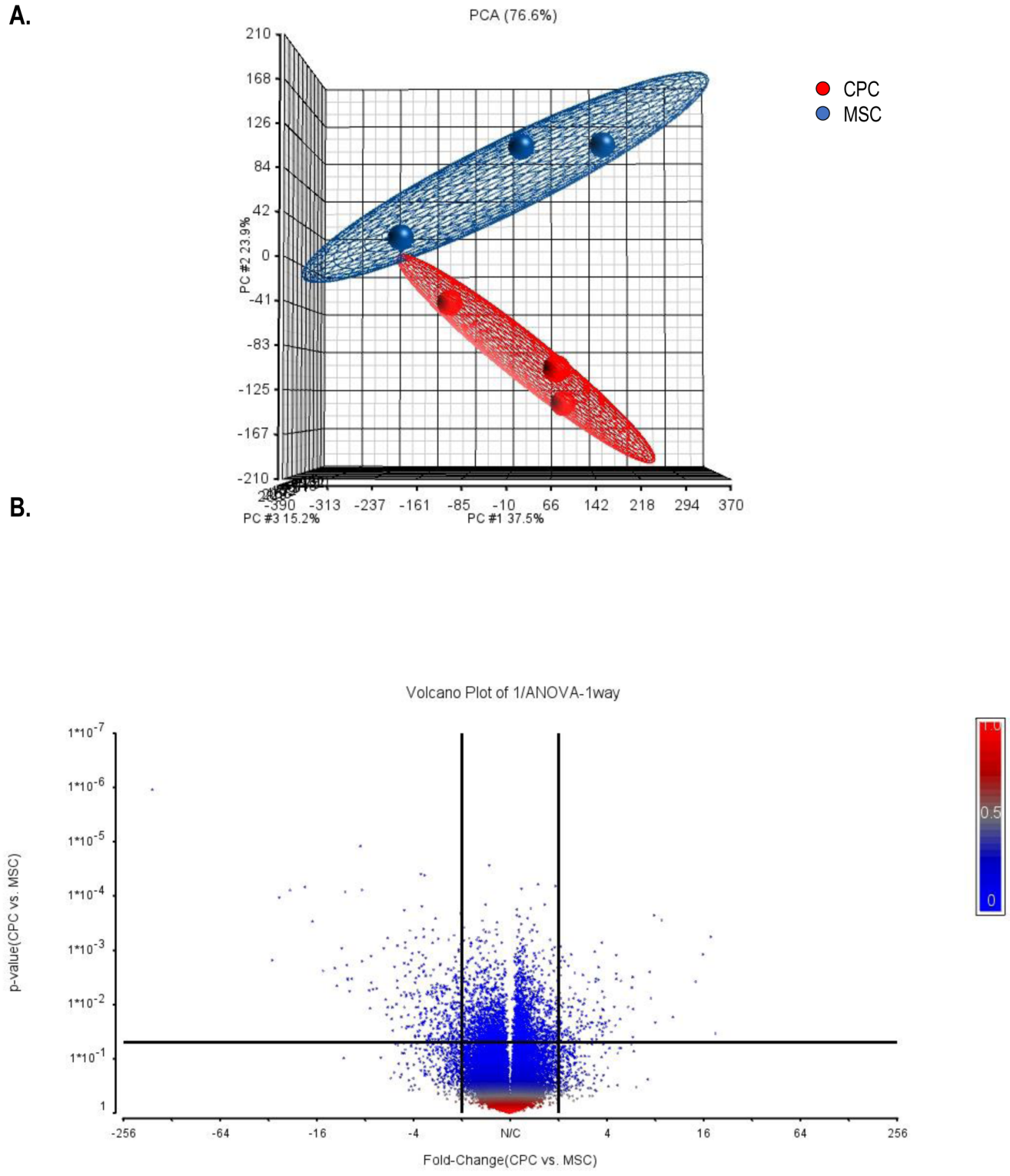

Figure 1

(A) Principal component analysis (PCA) showing transcriptomic differences between expression microarray data of both CPC and MSC cells. Each sample group is represented by a sphere and is colour-coded to indicate the corresponding cell type category. There is a clear difference in the transcriptomic

clustering between MSC and CPC samples. (B) Volcano plot showing fold-change and p-value for the comparison of CPC versus MSC cells. The vertical lines correspond to 2-fold up and down-regulation, respectively, and the horizontal line represent a P-value of < 0.05. Based on these parameters, the dots in the upper left and right quadrants represent differentially expressed genes with statistical significance.

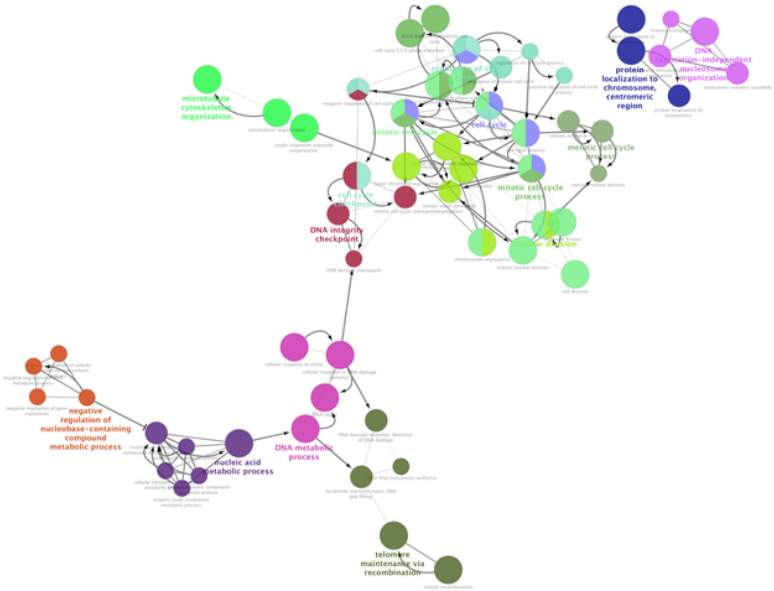

Figure 2

Over-represented GO Biological process terms after analysing the full list of differentially expressed genes between CPC and MSC cells. Circles represent the distinct terms, and arrows show the relationship between them. Terms related to cell cycle and DNA metabolism were enriched.

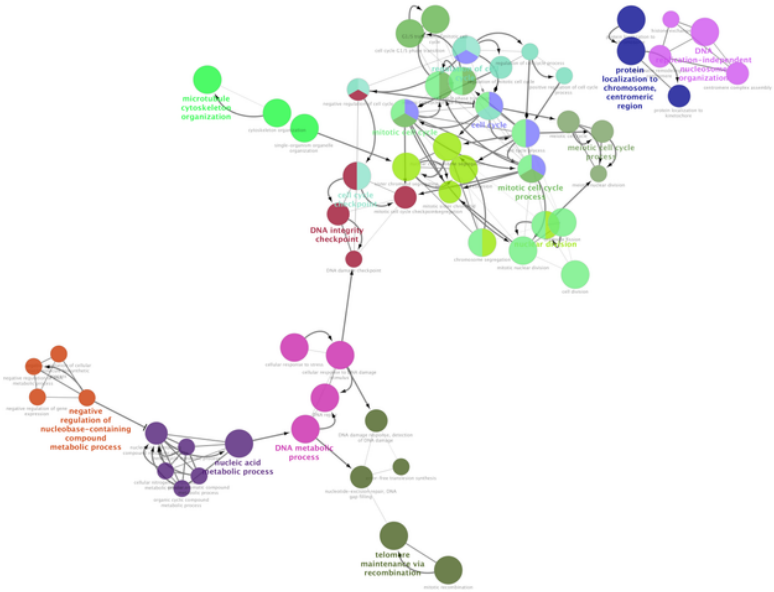

Figure 2

Over-represented GO Biological process terms after analysing the full list of differentially expressed genes between CPC and MSC cells. Circles represent the distinct terms, and arrows show the relationship between them. Terms related to cell cycle and DNA metabolism were enriched.

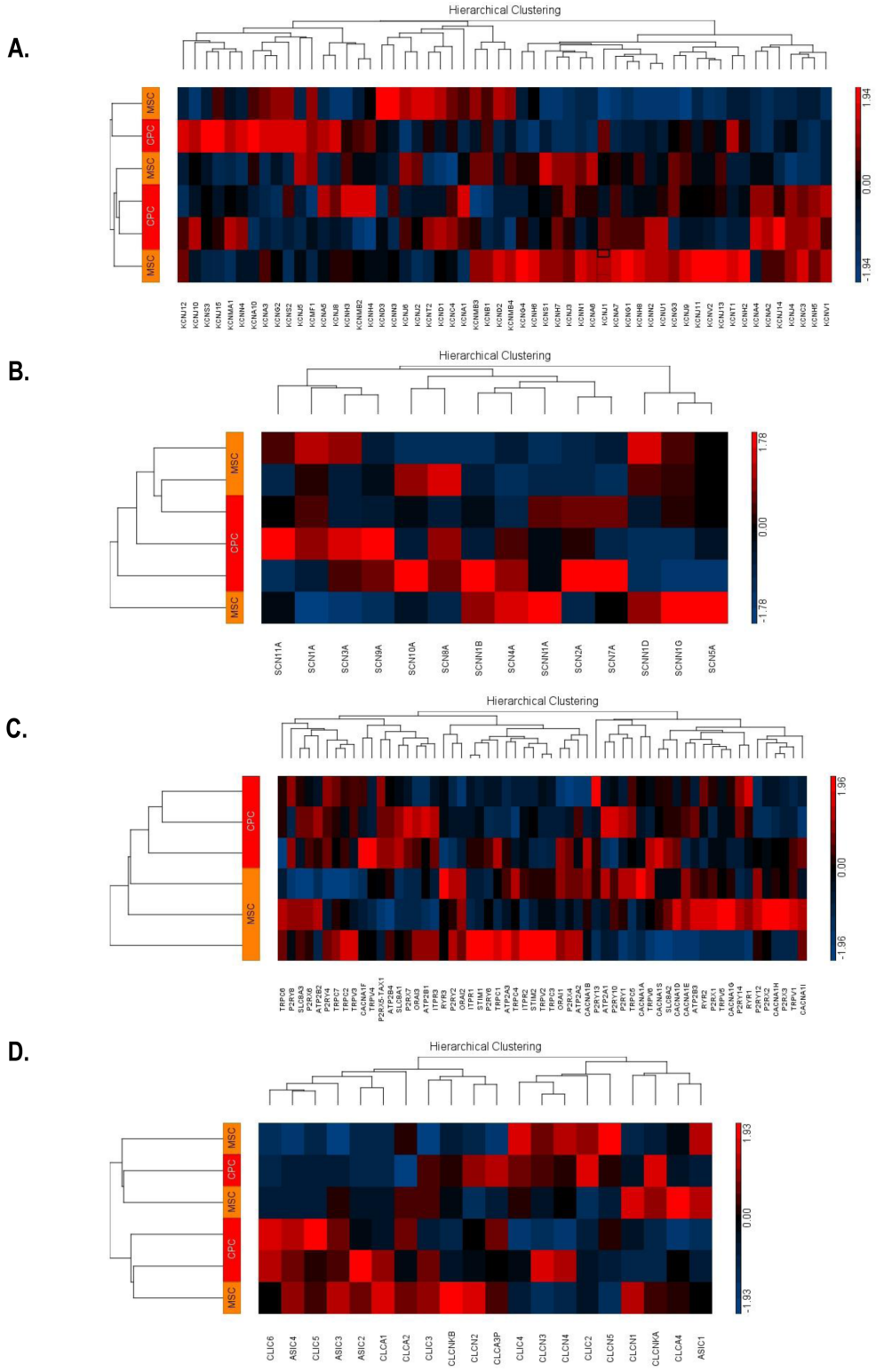

Figure 3

Heatmaps and hierarchical clustering dendrograms for genes coding for (A) potassium channel subunits, (B) sodium channel subunits, (C) proteins involved in mediating calcium homeostasis and other non-

selective ion channels, and (D) acid sensitive cation channels and chloride channels. Results are expressed as fold change of gene expression of CPC versus MSC cells. The red colour represents up regulation, grey colour indicates an unchanged expression, and blue colour represent down regulation of expression. The pattern and length of the branches in the dendrogram reflect the relatedness of the samples.

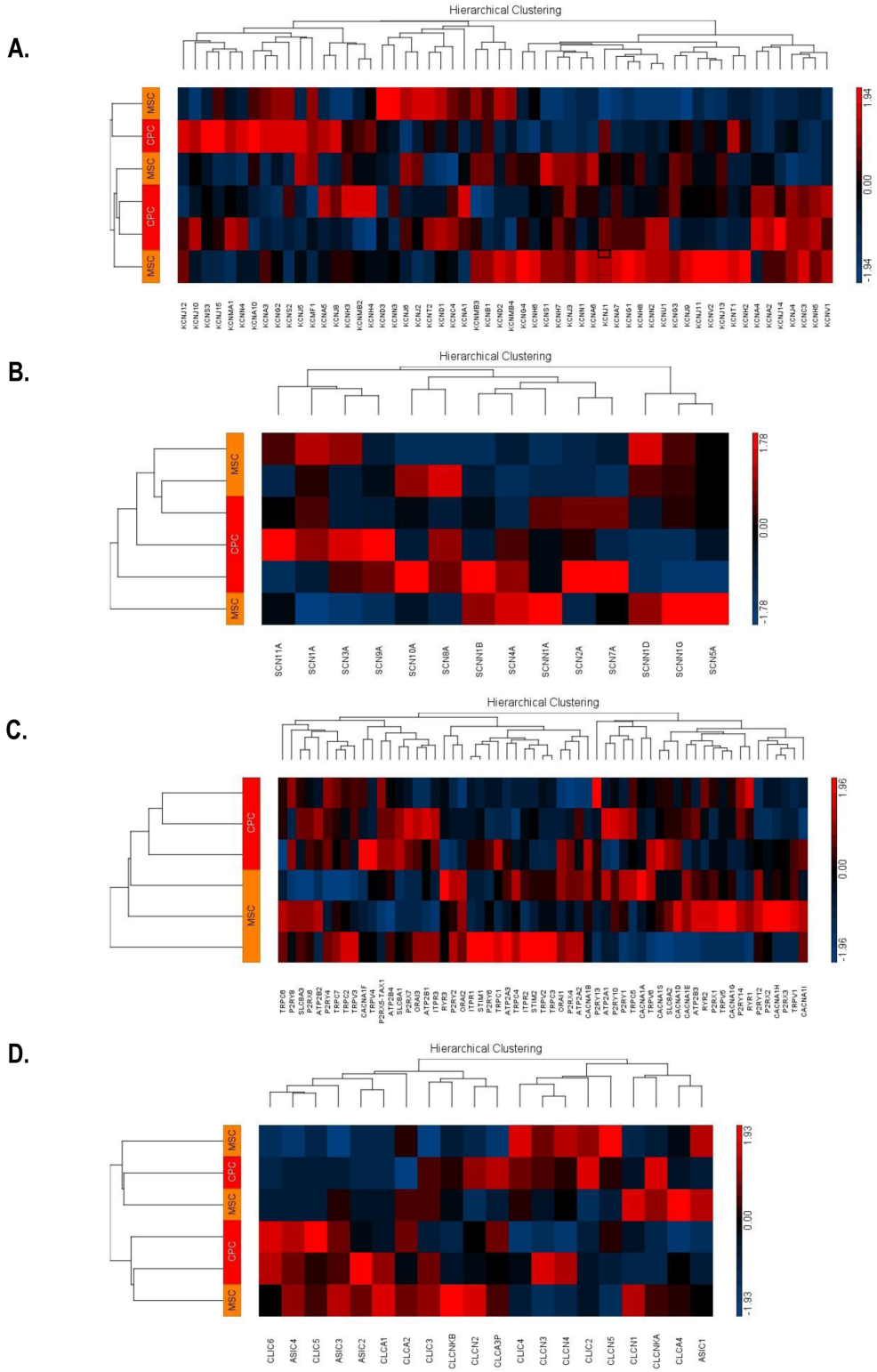

Figure 3

Heatmaps and hierarchical clustering dendrograms for genes coding for (A) potassium channel subunits, (B) sodium channel subunits, (C) proteins involved in mediating calcium homeostasis and other non-selective ion channels, and (D) acid sensitive cation channels and chloride channels. Results are expressed as fold change of gene expression of CPC versus MSC cells. The red colour represents up regulation, grey colour indicates an unchanged expression, and blue colour represent down regulation of expression. The pattern and length of the branches in the dendrogram reflect the relatedness of the samples.

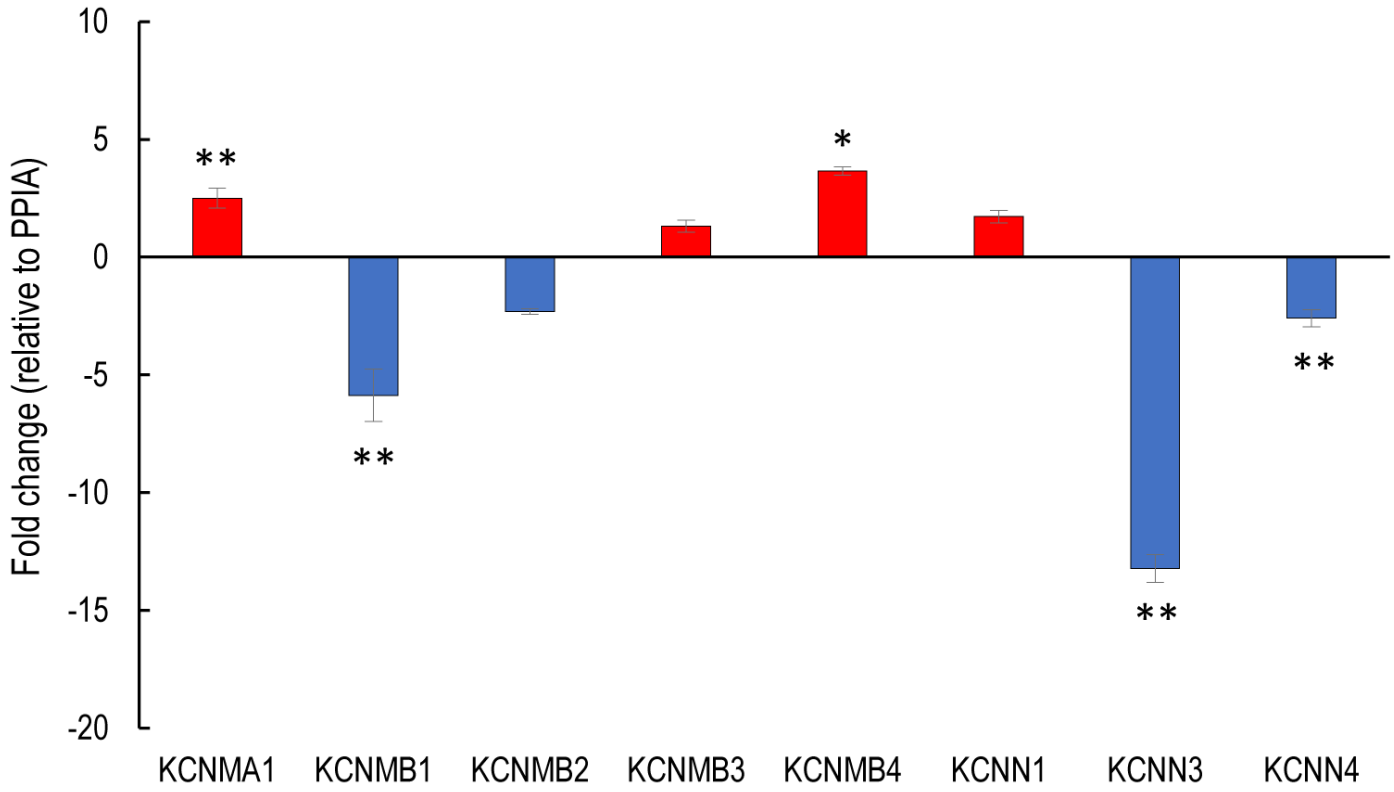

Figure 4

Transcript expression levels of selected genes coding for Ca2+ dependent potassium channel subunits as determined by RT-qPCR in CPC cells. Red bars represent up regulation, and blue bars represent down regulation of expression. Representative data (average ± SEM) out of 3 independent experiments (biological replicates) showing the same tendency of changes. Statistically significant (*P < 0.05; **P < 0.01) differences compared to MSCs are marked by asterisk(s).

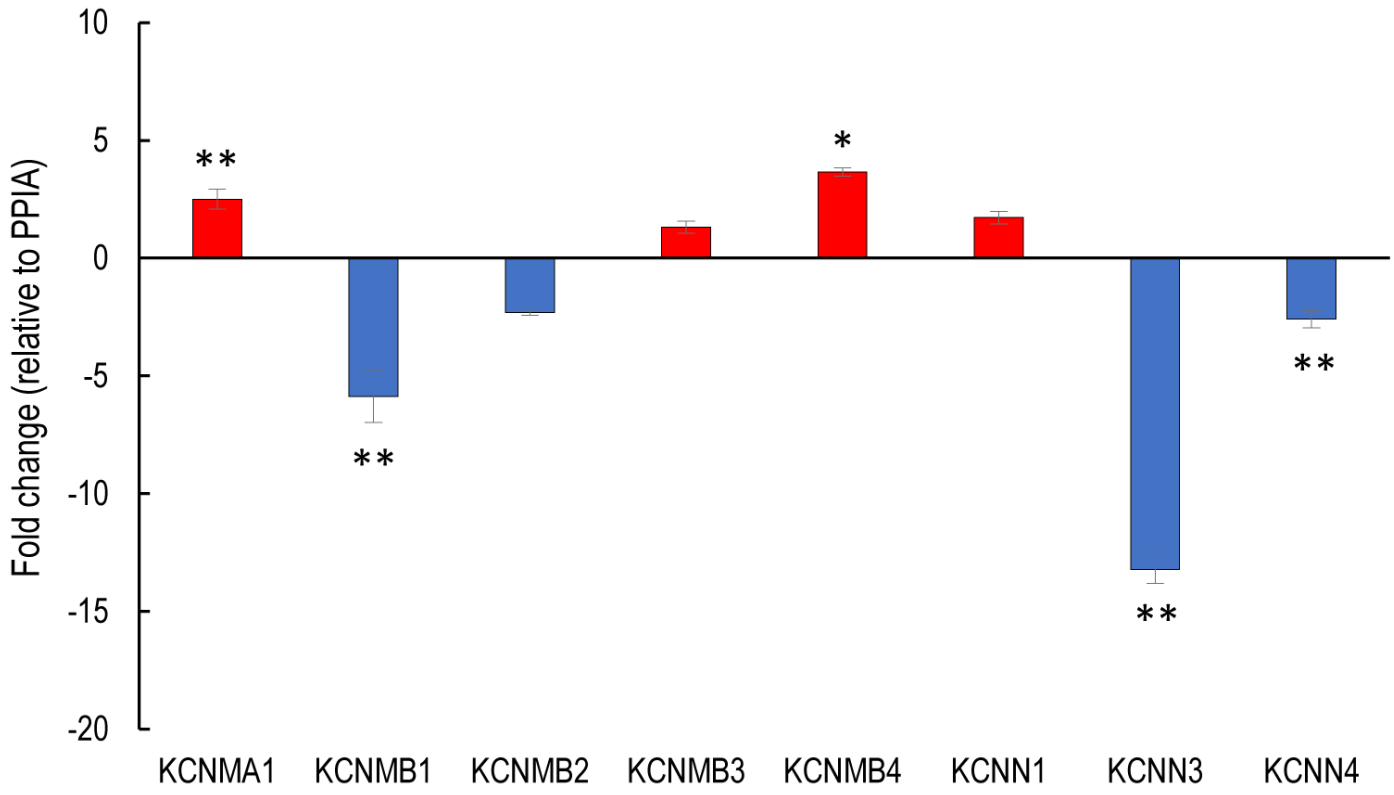

Figure 4

Transcript expression levels of selected genes coding for Ca2+ dependent potassium channel subunits as determined by RT-qPCR in CPC cells. Red bars represent up regulation, and blue bars represent down regulation of expression. Representative data (average ± SEM) out of 3 independent experiments (biological replicates) showing the same tendency of changes. Statistically significant (*P < 0.05; **P < 0.01) differences compared to MSCs are marked by asterisk(s).

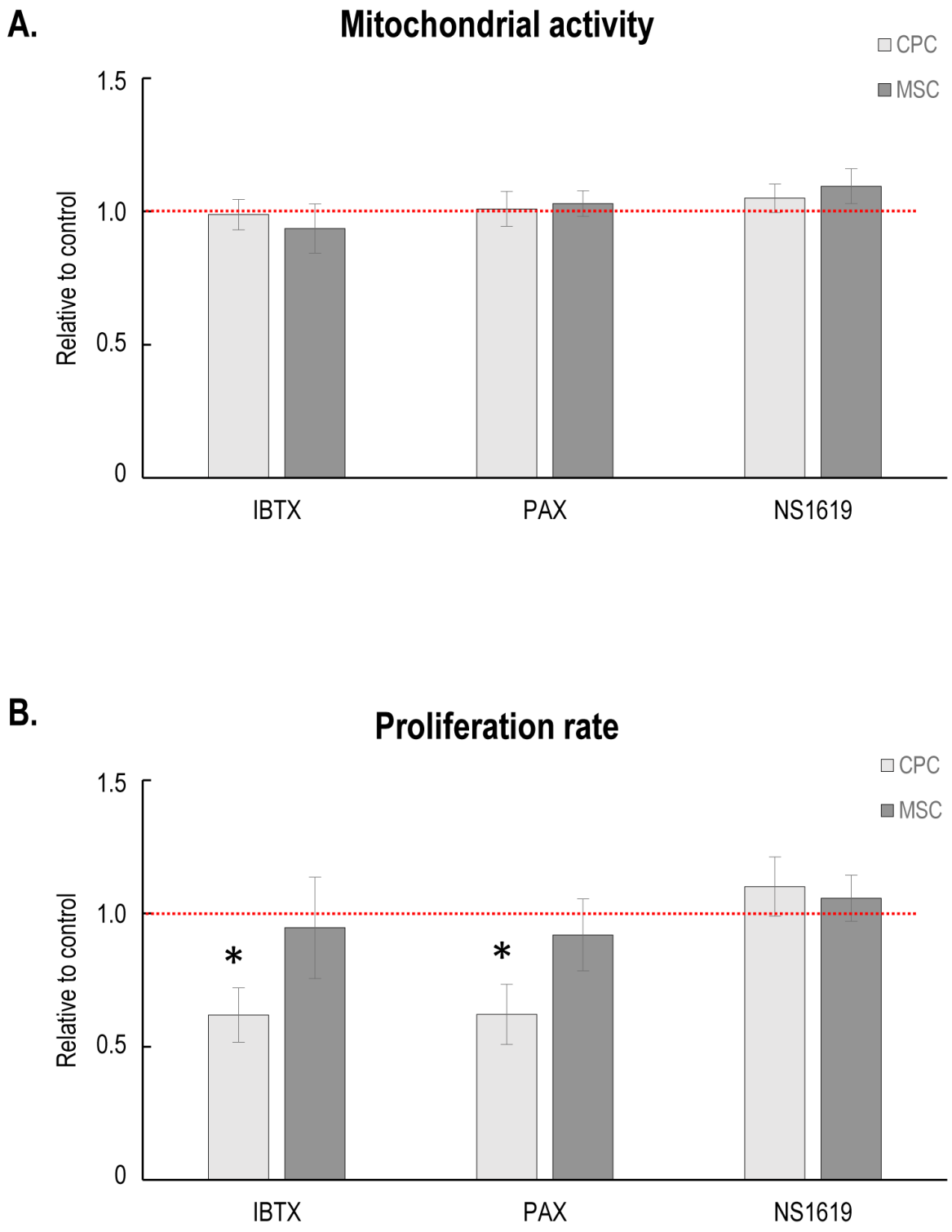

Figure 5

Mitochondrial activity, as a measure of cell viability (A) and proliferation rate (B) were determined by MTT test and 3H-thymidine incorporation assays, respectively, following pharmacological modulation of MaxiK channel function in CPC versus MSC. Representative data (average ± SEM) out of 3 independent experiments (biological replicates) showing the same tendency of changes. For each experimental group,

data were normalized to that of the respective vehicle control (not shown individually). Statistically significant (*P < 0.05) differences compared to the vehicle control are marked by asterisk.

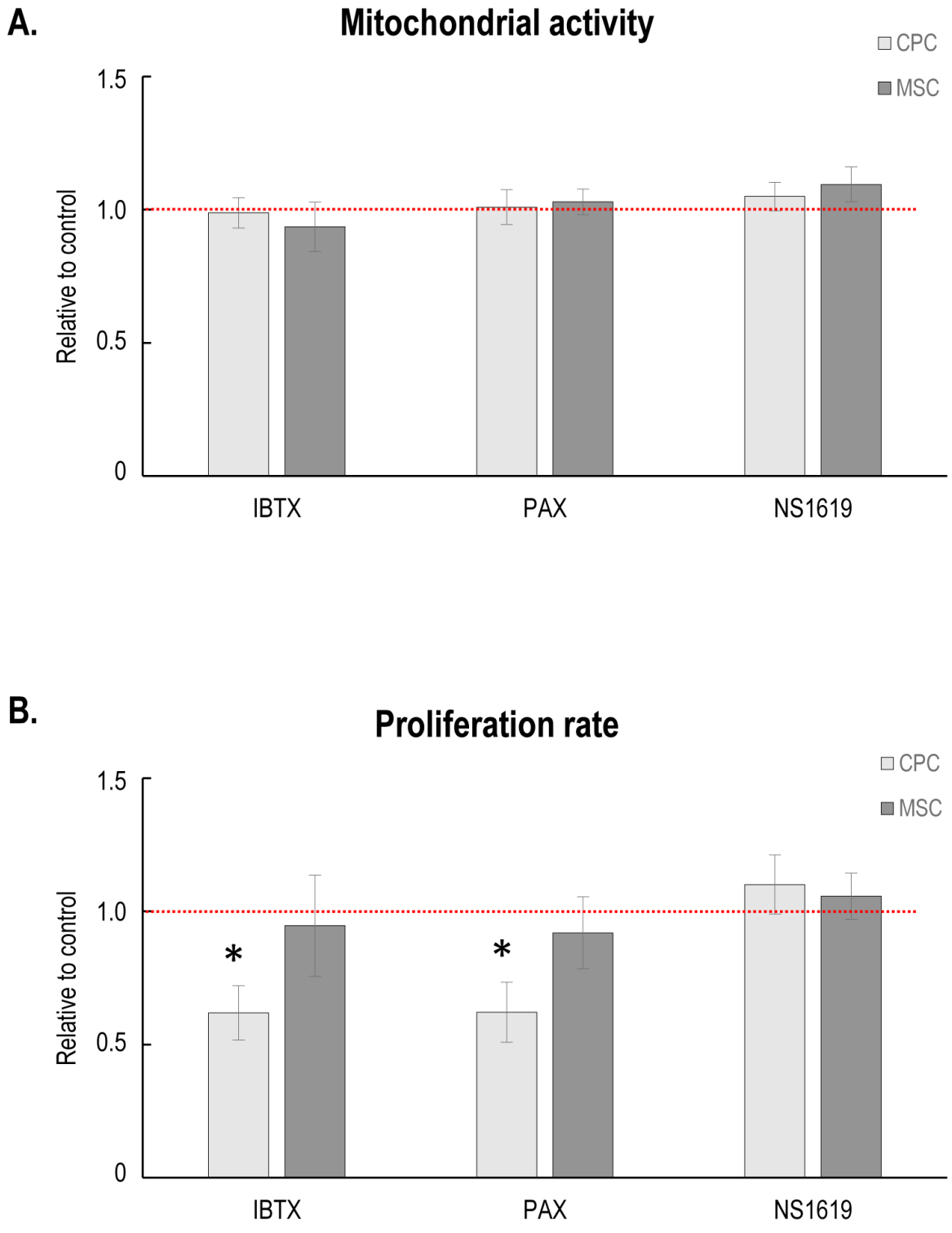

Figure 5

Mitochondrial activity, as a measure of cell viability (A) and proliferation rate (B) were determined by MTT test and 3H-thymidine incorporation assays, respectively, following pharmacological modulation of MaxiK channel function in CPC versus MSC. Representative data (average ± SEM) out of 3 independent

experiments (biological replicates) showing the same tendency of changes. For each experimental group, data were normalized to that of the respective vehicle control (not shown individually). Statistically significant (*P < 0.05) differences compared to the vehicle control are marked by asterisk.

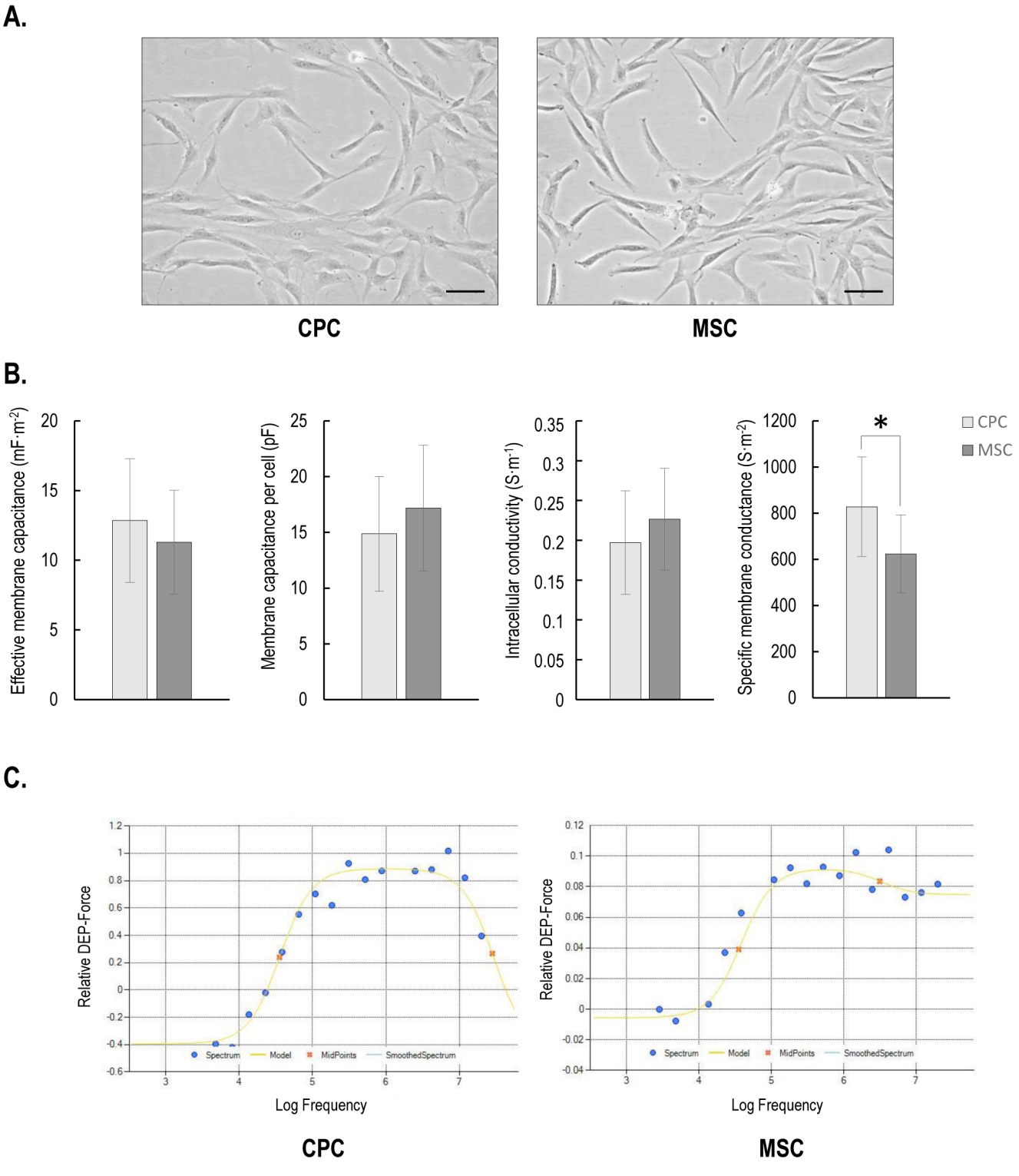

Figure 6

(A) Representative photomicrographs of CPC and MSC cell morphology prior to preparations for DEP measurements, showing typical mesenchymal cell morphology. Scale bar, 30 µm. (B) DEP parameters of

CPCs and MSCs. The effective membrane capacitance (CEff), intracellular conductivity and specific membrane conductance (GSpec) values were derived by fitting lines of best fit to DEP spectra and applying the ‘single-shell model’. Membrane capacitance per cell was calculated by multiplying the capacitance values with the average surface area of the cells. Error bars denote the standard deviations (SD). Each experiment was repeated three times. Asterisk denotes a statistically significant difference (*P < 0.05). (C) Examples of typical electrophysiological DEP (light intensity) spectra of CPCs (n=22) and MSCs (n=14) produced using the DEP-microwell, together with a ‘best-fit’ model from which the dielectric properties were determined. Changes in light intensity in the region of interest detected over a 60 s exposure were plotted against frequency (between 1.6 kHz–20 MHz). The spectra are negative at low frequencies, where cells are repelled from the electrodes; at higher frequencies the spectra become positive, where cells are being attracted to the electrodes. The spectra gradually increase until a plateau stage is reached. At higher frequencies still, the spectra begin to decrease (mainly for CPCs). Representative DEP spectra.

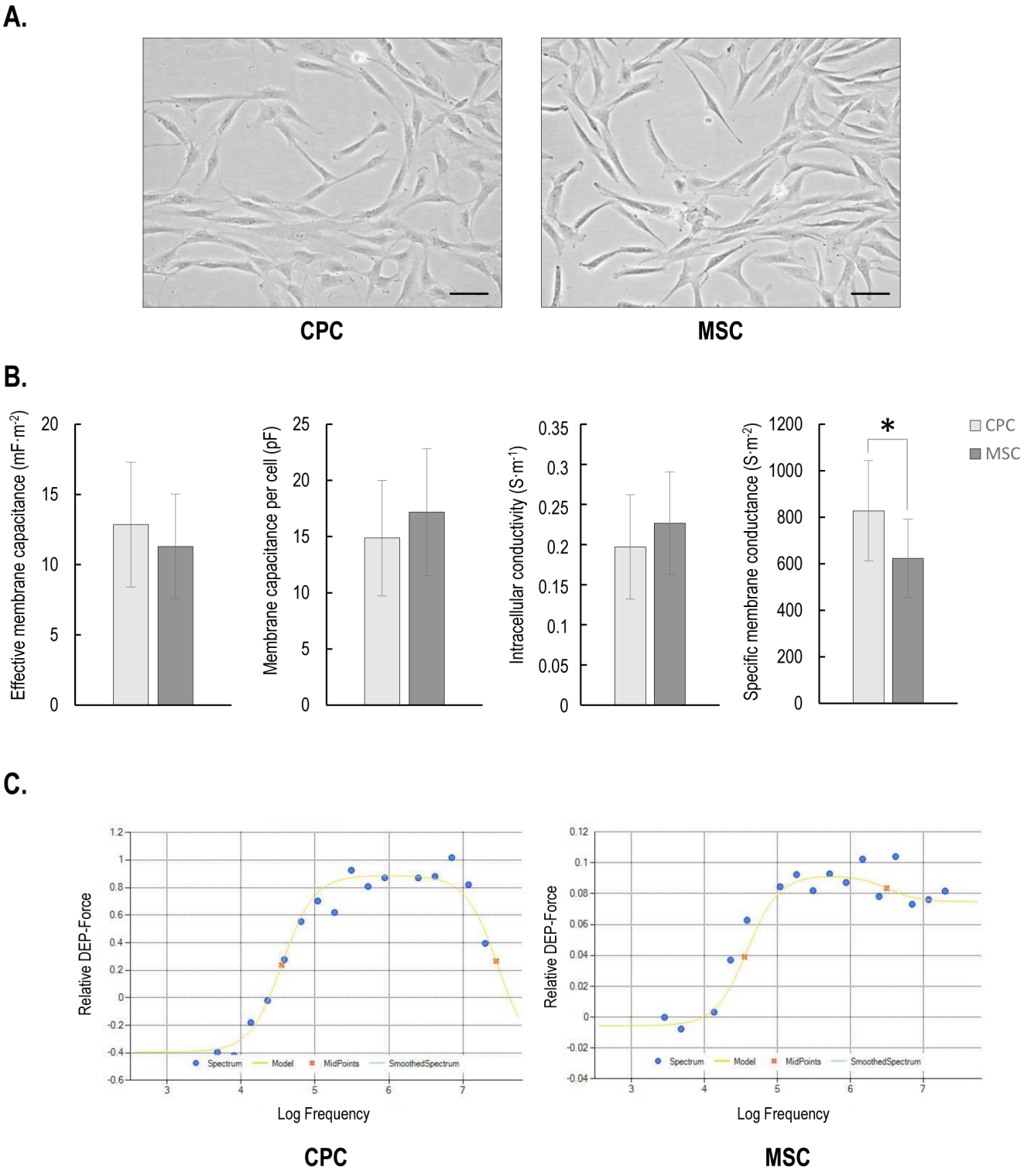

Figure 6

(A) Representative photomicrographs of CPC and MSC cell morphology prior to preparations for DEP measurements, showing typical mesenchymal cell morphology. Scale bar, 30 μm. (B) DEP parameters of CPCs and MSCs. The effective membrane capacitance (CEff), intracellular conductivity and specific membrane conductance (GSpec) values were derived by fitting lines of best fit to DEP spectra and applying the ‘single-shell model’. Membrane capacitance per cell was calculated by multiplying the

capacitance values with the average surface area of the cells. Error bars denote the standard deviations (SD). Each experiment was repeated three times. Asterisk denotes a statistically significant difference (*P < 0.05). (C) Examples of typical electrophysiological DEP (light intensity) spectra of CPCs (n=22) and MSCs (n=14) produced using the DEP-microwell, together with a ‘best-fit’ model from which the dielectric properties were determined. Changes in light intensity in the region of interest detected over a 60 s exposure were plotted against frequency (between 1.6 kHz–20 MHz). The spectra are negative at low frequencies, where cells are repelled from the electrodes; at higher frequencies the spectra become positive, where cells are being attracted to the electrodes. The spectra gradually increase until a plateau stage is reached. At higher frequencies still, the spectra begin to decrease (mainly for CPCs). Representative DEP spectra.

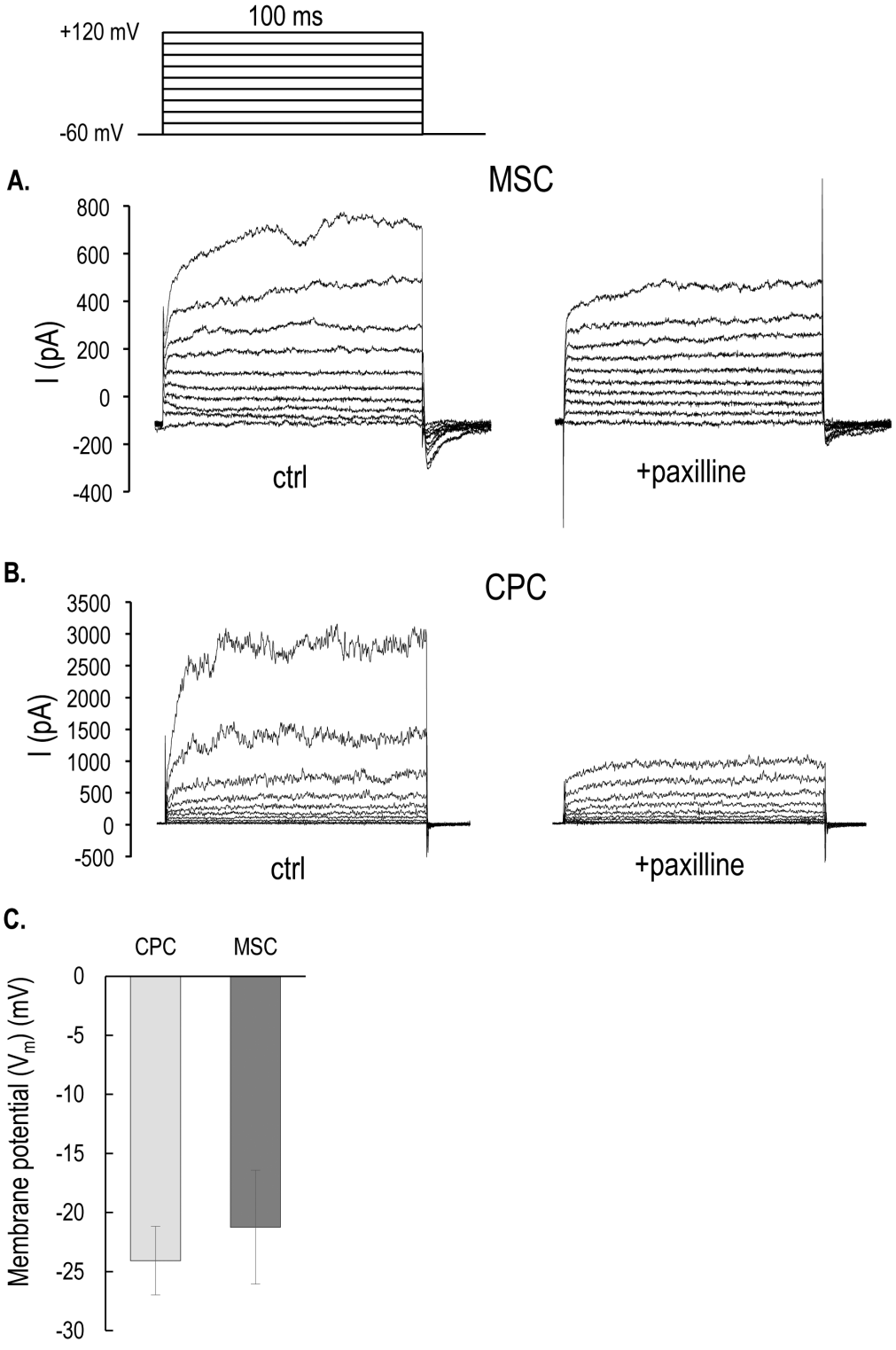

Figure 7

Whole-cell currents of MSC and CPC cells. Resting membrane potential was held at −60 mV. Current elicited by voltage step depolarizations between −40 and +120 mV are shown in MSC (A) and CPC (B) cells under control conditions and during paxilline treatment.

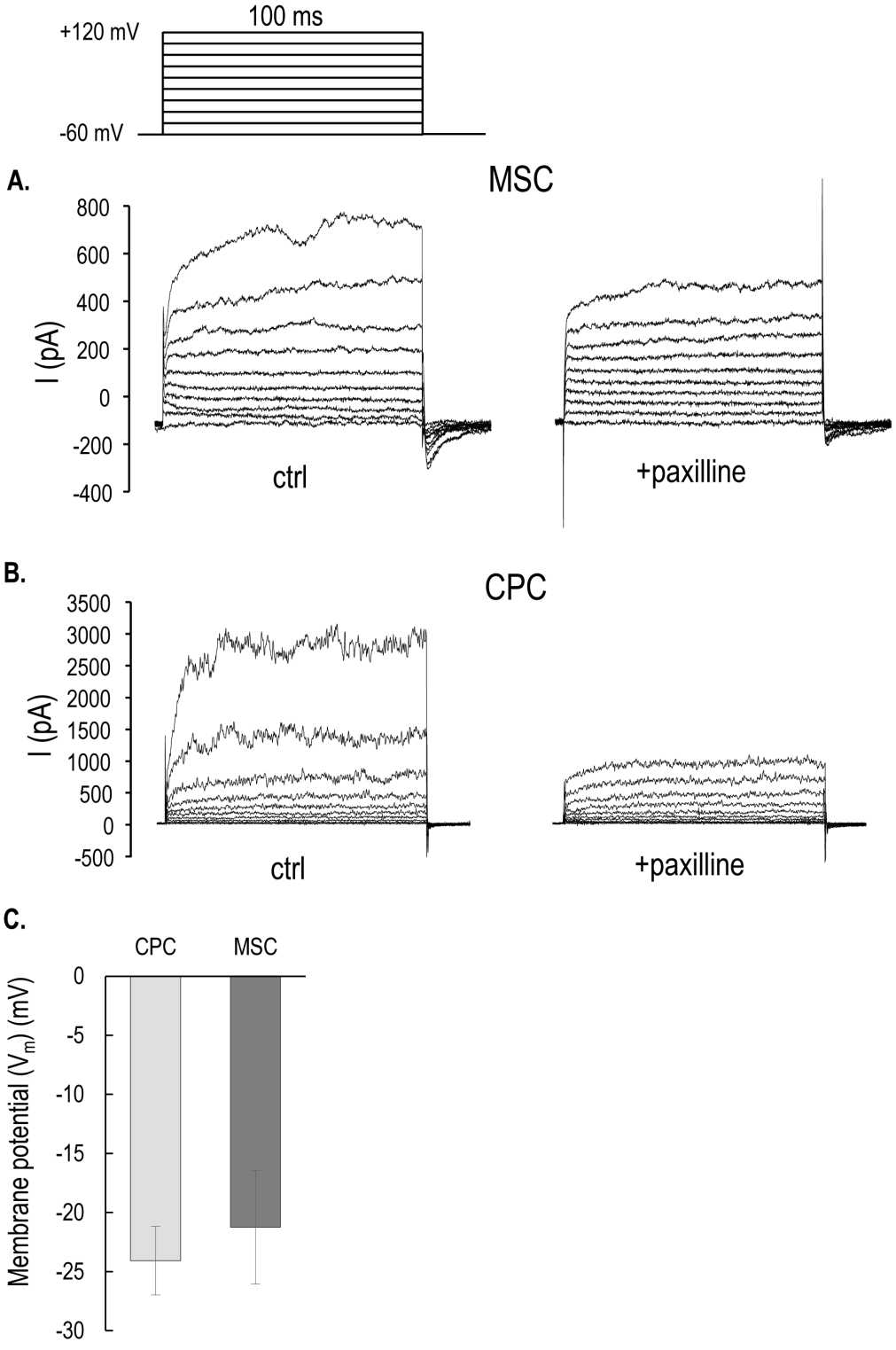

Figure 7

Whole-cell currents of MSC and CPC cells. Resting membrane potential was held at −60 mV. Current elicited by voltage step depolarizations between −40 and +120 mV are shown in MSC (A) and CPC (B) cells under control conditions and during paxilline treatment.

Supplementary Files

This is a list of supplementary files associated with this preprint. Click to download.

- supplementarymaterial.pdf
- supplementarymaterial.pdf
- supplementaryinformationproteomics.xlsx
- supplementaryinformationproteomics.xlsx